Secretion of IL1 by Dedifferentiated Melanoma Cells Inhibits JAK1-STAT3-Driven Actomyosin Contractility of Lymph Node Fibroblastic Reticular Cells

Christopher Rovera, Ilona Berestjuk, Margaux Lecacheur, Cassandre Tavernier, Serena Diazzi, Sabrina Pisano, Marie Irondelle, Aude Mallavialle, Jean Albrengues, Cédric Gaggioli, et al.

Secretion of interleukin-1 by dedifferentiated melanoma cells inhibits JAK1-STAT3-driven actomyosin contractility of lymph node fibroblastic reticular cells

Christopher Rovera[1,2], Ilona Berestjuk[1,2], Margaux Lecacheur[1,2], Cassandre Tavernier[1,2], Serena Diazzi[1,2], Sabrina Pisano[3], Marie Irondelle[1], Aude Mallavialle[1,2], Jean Albrengues[3], Cédric Gaggioli[3], Christophe A. Girard[1,2], Thierry Passeron[4,5], Marcel Deckert[1,2], Sophie Tartare-Deckert[1,2]*, Virginie Prod'homme[1,2]*

[1]Université Côte d'Azur, Inserm, C3M, Nice, France
[2]Team 11, Equipe labellisée Ligue Contre le Cancer, Nice, France
[3]Université Côte d'Azur, CNRS, Inserm, IRCAN, Nice, France
[4]Université Côte d'Azur, Inserm, C3M, Team 12, Nice, France
[5]Université Côte d'Azur, Department of Dermatology, CHU Nice, Nice, France

*Co-last authors

Running title: Dedifferentiated melanoma targets lymph node fibroblasts

Corresponding authors:

Virginie Prod'homme, Inserm UMR1065/C3M, 151 Route de Ginestière BP2 3194, F-06204 Nice cedex 3 France. Phone: 33 489 153 853; email: prodhomme@unice.fr

Marcel Deckert, Inserm UMR1065/C3M, 151 Route de Ginestière BP2 3194, F-06204 Nice cedex 3 France. Phone: 33 489 153 851; email: marcel.deckert@unice.fr

Conflict of interest: The authors declare no potential conflicts of interest.

Additional information:

Keywords: fibroblastic reticular cells, contractility, melanoma, interleukin-1, pre-metastatic niche

Word count: 6150 (main text), 255 (abstract)

Total number of figures: 8

Abstract

Fibroblastic reticular cells (FRC) are immunologically specialized myofibroblasts that control the elasticity of the lymph node (LN), in part through their contractile properties. Swelling of tumor-draining LN is a hallmark of lymphophilic cancers such as cutaneous melanoma. Melanoma displays high intratumoral heterogeneity with the coexistence of melanoma cells with variable differentiation phenotypes, from melanocytic to dedifferentiated states. Factors secreted by melanoma cells promote pre-metastatic LN reprograming and tumor spreading. Elucidating the impact of the melanoma secretome on FRC could help identify approaches to prevent metastasis. Here we show that melanocytic and dedifferentiated melanoma cells differentially impact the FRC contractile phenotype. Factors secreted by dedifferentiated cells, but not by melanocytic cells, strongly inhibited actomyosin-dependent contractile forces of FRC by decreasing the activity of the RHOA-ROCK pathway and the mechano-responsive transcriptional co-activator YAP. Transcriptional profiling and biochemical analyses indicated that actomyosin cytoskeleton relaxation in FRC is driven by inhibition of the JAK1-STAT3 pathway. This FRC relaxation was associated with increased FRC proliferation and activation and with elevated tumor invasion in vitro. The secretome of dedifferentiated melanoma cells also modulated the biomechanical properties of distant LN in pre-metastatic mouse models. Lastly, interleukin-1 produced by dedifferentiated cells was involved in the inhibition of FRC contractility. These data highlight the role of the JAK1-STAT3 and YAP pathways in spontaneous contractility of resting FRC. They also suggest that dedifferentiated melanoma cells specifically target FRC biomechanical properties to favor tumor spreading in the pre-metastatic LN niche. Targeting this remote communication could be an effective strategy to prevent metastatic spread of the disease.

Statement of significance

Communication between dedifferentiated melanoma cells and lymph node fibroblasts reprograms the biomechanical properties of the pre-metastatic lymph node niche to promote tumor invasion.

Introduction

Melanoma is a very aggressive skin cancer due to its high propensity to metastasis and pronounced intratumor heterogeneity. Four genomic subtypes of cutaneous melanoma have been defined based on the mutational pattern in *BRAF*, *RAS*, *NF1*, or none of these (1). During metastatic progression, melanoma cells are highly plastic and dynamically switch between proliferative and invasive phenotypes associated with distinct differentiation states ranging from melanocytic to dedifferentiated (2-5). The proliferative melanocytic state is characterized by high expression of the melanocyte lineage-specific Microphthalmia-Associated Transcription Factor (MITF) and low expression of the tyrosine kinase receptor AXL, whereas the invasive dedifferentiated state shows low expression of MITF and high expression of AXL. Dedifferentiated melanoma cells display a mesenchymal-like phenotype associated with drug resistance (6-8). Whether the melanocytic and dedifferentiated melanoma cell populations differ in their ability to communicate with the metastatic stromal host niche remains poorly understood.

Cutaneous melanoma is a cancer with an inherent potential for lymph node (LN) colonization, an event contributing to systemic metastasis (9-11). Melanoma cells secrete extracellular vesicles (12) and soluble factors (13) migrating to the pre-metastatic LN and conditioning immune cells (14), lymphatic endothelial cells (13,15) and fibroblastic reticular cells (FRC) (16). This reprogramming of the LN microenvironment creates a favorable niche that supports metastatic development.

FRC are immunospecialized myofibroblasts of lymphoid organs characterized as $CD31^{-}Podoplanin^{+}$ (PDPN) mesenchymal cells. They form a network in close contact with T cells and dendritic cells (DC) in the LN paracortical area and regulate immune cell recruitment, survival and activation (17). With a notable spontaneous contractibility (18-20) and the secretion and remodeling of a dense reticular network of conduits (17,20), FRC control the LN elasticity and microarchitecture. PDPN was shown to drive the actomyosin contractility of FRC through its binding to proteins of the ezrin, radixin and moesin (ERM) family, leading to RHOA activation (18,19,21,22). During an immune response, migratory DC expressing high levels of C-type lectin-like receptor 2 (CLEC2) are recruited to the LN. CLEC2 binding to PDPN on FRC dismantles the

PDPN-ERM interaction, inhibiting actomyosin contractility and resulting in FRC stretching allowing rapid LN expansion (18,19).

In other tissues, like the skin, quiescent fibroblasts are not spontaneously contractile but can be converted into contractile myofibroblasts by factors secreted during wound healing or tumor progression, such as TGF-β or IL-6 family cytokines (23). Factors secreted by tumor cells transform fibroblasts in the tumor vicinity into cancer associated fibroblasts (CAF) (24). CAF are characterized by a contractile phenotype and the high expression of markers like α-smooth muscle actin (α-SMA, *ACTA2* gene), platelet derived growth factor receptor-α (PDGFR-α) and PDGFR-β, fibroblast activation protein α (FAP), fibroblast-specific protein-1 (FSP1, *S100A4* gene), fibronectin (FN) and a FN isoform containing the EDA domain (EDA-FN), vimentin (VIM) or secreted protein acidic and rich in cysteine (SPARC) (24). In CAF, actomyosin contractility is driven by RHO and RHO-kinase (ROCK) signaling, leading to an increased phosphorylation of the myosin light-chain 2 (MLC2) (25), and by the activation of the mechano-responsive yes1 associated transcriptional regulator (YAP) (26,27). Cytokines from the IL-6 family (IL-6, LIF, OSM) have been shown to induce RHO-ROCK-dependent CAF contractility through the GP130 (IL6ST)-JAK1-STAT3 pathway (28,29). TGF-β increases actomyosin contractility in fibroblasts by promoting LIF expression, which subsequently epigenetically activates JAK-STAT signaling (30). Actomyosin contraction in CAF is associated with cell shape remodeling, increased F-actin stress fibers and drives force-mediated extracellular matrix remodeling (25,26).

Malignant LN colonization is preceded by pre-metastatic LN swelling (15,16,31) but it remains incompletely understood whether (and how) tumor-derived cues alter FRC specific contractile properties during pre-metastatic niche reprogramming. In this study, we characterized the impact of factors secreted by melanocytic or dedifferentiated melanoma cells on the actomyosin contractility of isolated human FRC and in murine pre-metastatic LN models, and identified the underlying signaling pathways, the responsible tumor factors as well as the impact of this process on the metastatic properties of tumor cells.

Materials and Methods

Isolation and culture of primary fibroblasts and CAF

Primary human LN Fibroblasts (LN-F) (#2530, ScienCell) were amplified in Fibroblast Medium (#2301, ScienCell) supplemented with 1% Fibroblast Growth Supplement (#2352, ScienCell), 10% FBS (Gibco) and 100 µg/ml Penicillin/Streptomycin solution (P/S, Gibco). Skin Fibroblasts (Skin-F) from healthy donors were isolated as described previously (32). CAF were isolated as described previously (33) from melanoma skin or LN clinical specimens (n = 9) obtained with written informed consent from patients, in accordance with the Declaration of Helsinki. The study was approved by local ethic committees (Nice Hospital Center and University Côte d'Azur). Skin-F and CAF were cultured in DMEM with 100 µg/ml P/S and 10% FBS. Fibroblasts were starved for 5 to 7 days in DMEM 0.5% FBS (control medium) before any experiment and were then stimulated every two days with control medium or melanoma CM supplemented with 0.5% FBS. They were used until passage 10. In some experiments, cells were treated with 2 ng/ml TGF-β1 (#11343160, ImmunoTools), 2 ng/ml LIF (#300-05, PeproTech), 2 ng/ml IL-1α (#200-01A, PeproTech), 2 ng/ml IL-1β (#200-01B, PeproTech) or 10 µM Ruxolitinib (#S1378, Selleckchem), 10 µM Y-27632 (#S1049, Selleckchem) or 10 µM SB431542 (#S1067, Selleckchem). All experiments were performed on plastic, except collagen gel contraction assays and immunostainings.

Melanoma cell culture

Human melanoma cell lines were obtained as previously described (6,34-36). They were authenticated by short tandem repeat DNA profile genotyping (Eurofins Genomics). Fluorescent 1205Lu Red cells were previously described (33). Short-term cultures of patient melanoma cells MM001, MM029, MM074 and MM099 were kindly provided by J.-C. Marine (8) and MNC1 were described previously (36). Human melanoma cells were cultured in DMEM supplemented with 7% FBS and used until passage 30. Mouse YUMM1.7 cells (RRID: CVCL_JK16) were kindly provided by M. Bosenberg (37). They were cultured in Opti-MEM supplemented with 3% FBS. All cells were routinely tested for the absence of mycoplasma by PCR.

Conditioned media (CM)

Melanoma cells at 80% confluence were cultured for 24h in FBS-free medium. The culture supernatant was filtered (0.45 µM) to remove cellular debris. CM prepared from 501Mel and 1205Lu melanoma cells were analyzed by mass spectrometry and antibody array as described (35,36). CM injected to mice were previously concentrated 10-fold on 3 kDa MW cut-off membrane (Amicon Ultra-4, Merck Millipore). The resulting CM, or EVs, were aliquoted and frozen at -80°C until used.

Collagen gel remodeling assays

Fibroblasts ($7x10^3$ cells) were embedded in 30 µl of a 3.5 mg/ml collagen I (#354249, Corning) and 2 mg/ml Matrigel (#E1270, Sigma) mix and seeded in 5 mm Glass Diameter coverslip 96-well plate (#P96G-1.5-5-F, MatTek). Once the gel was set (30 min at 37°C), it was overlaid with 100 µl medium. Gels were photographed every 1 to 3 days to measure their area with ImageJ software (RRID: SCR_003070). The percentage of gel contraction was calculated as followed: 100 - 100 x (gel area / well area).

Atomic force microscopy (AFM)

Mechanical properties of LN-F-remodeled collagen gels and unfixed 10 µm frozen LN sections were analyzed by AFM (see supplementary data for details).

Proliferation assays

LN-F proliferation was measured using the CellTiter 96 Aqueous Non-Radioactive Cell Proliferation kit (#G5421, Promega) according to the manufacturer's instructions, or by cell counting, and was normalized to the control medium condition.

Flow cytometry

Cells were washed in PBS and incubated at 4°C for 30 min in PBS 2% FBS, 2 mM EDTA with antibodies and control isotypes listed in supplementary Table 1. Then, cells were washed in PBS and analyzed with BD FACSCANTO II cytometer (BD Biosciences) and the FlowJo software (RRID: SCR_008520). A minimum number of

$5x10^3$ relevant LN-F were analyzed after exclusion of dead cells (SSC-H/FSC-H gate) and doublets (FCS-A/FSC-H gate).

RNAi studies

Transfection of siRNAs listed in supplementary Table 2 was carried out using Lipofectamine RNAiMAX (#13778150, ThermoFisher) at a final concentration of 50 nM. Cells were assayed at 2 days post transfection.

Real-time quantitative PCR

Total RNAs were extracted using NucleoSpin RNA Plus kit (#740984.50, Macherey-Nagel). Reverse transcription was performed with the High-capacity cDNA Reverse Transcription kit (#4368814, Applied Biosystems). Quantitative PCR was performed using the Platinum SYBR Green qPCR Supermix (#11558656, FisherScientific) with the StepOnePlus System (Applied Biosystems). Relative mRNA levels were determined using the $2\Delta\Delta C_t$ method and *ACTB, GAPDH, HPRT* and *PPIA* as housekeeping genes.

Microarray experiment and analysis

LN-F were cultured for 48h with control medium or 1205Lu CM in 4 different experiments. RNAs were then extracted as described above and analyzed on SurePrint G3 Human Gene Expression 8x60K v2 Microarrays (#G4851B, Agilent Technologies) as previously described (38) (see supplementary data for details).

Immunoblots

Immunoblot were realized as previously described (36) with antibodies listed in supplementary Table 1.

RHOA assays

RHOA activity was measured on LN-F lysates using the RHOA G-LISA Activation Assay kit (#BK124, Cytoskeleton). Data are the mean ± SEM of arbitrary units of RHOA activity.

Immunofluorescence

LN-F were grown 4 days on coverslips coated with 20 µg/cm^2 collagen or on synthetic hydrogels of 2.8 kPa or 0.2 kPa stiffness coated with 20 µg/cm^2 collagen. Hydrogels were prepared as previously described (39) (see supplementary data for details). Then, cells were fixed in 4% paraformaldehyde, permeabilized in 0.3% Triton, blocked in 0.1% Triton, 5% Goat Serum and stained overnight at 4°C with primary antibodies (supplementary Table 1) diluted in 0.1% Triton, 2% Goat Serum. Following incubation with Alexa Fluor-conjugated secondary antibodies (1:1000, ThermoFisher) and Texas Red- or Alexa Fluor 488-conjugated Phalloidin (1:200, ThermoFisher), nuclei were stained with Hoechst (#H1399, ThermoFisher) and coverslips were mounted in ProLong diamond antifade (#P36961, ThermoFisher). Images were acquired on a wide-field microscope (Leica DM5500B, 40X magnification) or a confocal microscope (Nikon Eclipse Ti, 20X or 40X magnification). Images were analyzed with the ImageJ software to quantify the cell shape index, the mean fluorescence per cell (Integrated density) and the nuclear/cytosolic ratio of YAP.

Mouse model of premetastatic draining LN

Experiments with mice were approved by a IACUC under project license APAFIS#21820-2019070916066283v4. Female athymic nude mice (Charles River, RRID:IMSR_CRL:490) or immune competent 8-week-old C57BL/6j mice (Janvier, RRID: IMSR_JAX:000664) were injected every other day with 15 µl of 1205Lu or YUMM1.7 CM in the dermis of the right ear and 15 µl of 501Mel CM or control medium in the left ear. At day 7, mice were sacrificed and the superficial parotid draining LN were harvested for subsequent analysis. LN of the same mouse were compared for paired statistical analysis. LN were fixed overnight at 4°C with 3% paraformaldehyde (except LN prepared for AFM), soaked in 30% sucrose, and embedded in OCT compound (#4583-01, Gentaur). Frozen sections (10 µm) were then treated as described in the Immunofluorescence section. Z-stack images were captured every 0.5 µm on a confocal microscope (Nikon Eclipse Ti, 60X magnification). 3D-reconstituted images were analyzed with the ImageJ software to quantify the nuclear/cytosolic ratio of YAP.

Collagen gel invasion assays

LN-F ($2.3x10^4$) were embedded in 100 µl of 2.5 mg/ml collagen I and 2 mg/ml Matrigel mix and seeded inside 24-well cell culture inserts (8 µm pore size, #3422, Corning). Once the gels were polymerized, the chambers were filled with control medium (with IL-1β or Y-27632) or melanoma CM. The medium was changed on day 2. All conditions were performed in triplicates. On day 5, the LN-F remodeled collagen gels were washed twice, and gaps around contracted gels were filled with collagen/Matrigel mix. Then, 10^5 1205Lu Red cells were seeded on top of the gels in DMEM and the lower chamber was filled with DMEM 20% FBS. After 3 days, the collagen gels were placed upside down on glass-bottom dishes (#80136, Ibidi). Z-stack images were captured every 10 µm over 200 µm, on an inverted confocal microscope (Nikon Eclipse Ti, 20X magnification). The number of cells in each 10 µm-step image was analyzed with ImageJ software and normalized to the number of cells detected in the stack. Maximum distance of invasion was defined as the z value above which 5% of cells in the stack was found. 3D projections were obtained with the NIS-Elements software (Nikon).

Statistical analysis

Statistical analysis was performed using Prism (v 8, GraphPad, RRID: SCR_002798). Unpaired two-tailed Mann-Whitney tests were used for statistical comparisons between two groups and Kruskal-Wallis tests with Dunn's post-tests or two-way analysis of variance (ANOVA) tests with Sidak's post-tests to compare three or more groups. Histogram plots and curves represent mean ± SEM and Violin plots represent median +/- quartiles. P values ≤ 0.05 were considered statistically significant.

Data availability

The experimental data from microarray have been deposited in the NCBI Gene Expression Omnibus (GEO) database (RRID: SCR_005012) under the series record GSE157355.

Results

LN fibroblasts harbor a CAF-like phenotype associated with spontaneous cell contractility.

To investigate the interactions between melanoma cells and FRC, we employed primary fibroblasts isolated from human LN. Because several mesenchymal subsets coexist in the LN (20,40), we first characterized these primary LN fibroblasts (LN-F) using microarray profiling, qRT-PCR, and flow cytometry (Supplementary Fig. S1A-C). Markers expressed by LN-F were typical of FRC (*PECAM1*$^{-}$, *PDPN*$^{+}$, *CR2*$^{-}$, *MADCAM1*$^{-}$), the most abundant LN mesenchymal subset.

FRC exhibit spontaneous contractility (18-20). When embedded in a collagen gel, LN-F isolated from 4 different donors demonstrated basal force-mediated gel remodeling, driven by the ROCK-actomyosin pathway, and inhibited by the ROCK inhibitor Y-27632 and the myosin inhibitor blebbistatin (**Fig. 1A** and supplementary Fig. S1D-E). LN-F displayed the same high propensity to drive collagen gel remodeling as primary CAF isolated from skin or LN melanomas (**Fig. 1B**). However, primary skin fibroblasts (skin-F) were not able to contract the collagen gel unless activated with TGF-β to a CAF-like phenotype. In contrast, LN-F spontaneous contraction was not modulated by TGF-β. As for LN-F, contractile properties of TGF-β-activated skin-F and CAF were dependent of the ROCK-actomyosin pathway and inhibited by Y-27632. In agreement with the collagen gel remodeling results, LN-F contractile activity was associated with higher basal levels of F-actin stress fibers and YAP nuclear localization compared to skin-F (**Fig. 1C** and **D**). However, in contrast to skin-F, F-actin fibers and YAP nuclear localization were not increased by TGF-β treatment in LN-F. qRT-PCR analysis revealed that several CAF markers like *ACTA2* (α-SMA), *FAP*, *EDA-FN* or *SPARC* were highly expressed in LN-F compared to skin-F, suggesting that resting LN-F share many properties with CAF (**Fig. 1E**). Immunoblot analysis also showed TGF-β-independent high expression of FN, PDGFR-β, FAP and α-SMA in resting LN-F, to levels equivalent or higher than TGF-β-activated skin-F (**Fig. 1F**). This is consistent with the notion that high α-SMA expression is associated with fibroblast contractility (41). Collectively, these results validate the FRC signature of LN-F and unveil that quiescent LN-F display some phenotypic and functional properties of CAF. Our aim

was then to investigate whether, and how, melanoma cells modulate the contractile properties of fibroblasts in the LN metastatic niche.

Factors secreted by dedifferentiated melanoma cells with a MITF^{low} AXL^{high} signature inhibit LN-F contractility.

Melanoma cells harbor transcriptional states ranging from melanocytic (MITF^{high} AXL^{low}) to dedifferentiated (MITF^{low} AXL^{high}) (2-5). To compare the ability of these melanoma subpopulations to modulate LN-F contractility, we selected cell lines as well as short-term cultures of melanoma patients, either melanocytic (501Mel, MeWo, SK-MEL-28, WM164 and MM001, MM074) or dedifferentiated (1205Lu, WM793, WM2032, SBcl2 and MNC1, MM029, MM099), whose expression of MITF and AXL genes was analyzed by qRT-PCR (Supplementary Fig. S2A). Then, to model melanoma distant reprogramming of FRC in the pre-metastatic LN, we treated LN-F with conditioned medium (CM) harvested from melanoma cell cultures and containing the factors secreted by melanoma cells. Tumor cell-derived factors, like TGF-β, are known to induce fibroblast actomyosin contraction, as during CAF differentiation (24). Strikingly, CM secreted by dedifferentiated melanoma cells drastically inhibited the spontaneous ability of LN-F to contract collagen gels, while CM from melanocytic melanoma cells had no effect (**Fig. 2A**). The ability of melanoma cells to inhibit LN-F contractility was indeed strongly inversely correlated to their MITF expression (**Fig. 2B**). To get a more comprehensive view of the effect of factors secreted by melanocytic or dedifferentiated melanomas on LN-F reprogramming, we carried out the study with two representative melanoma cell lines displaying the melanocytic MITF^{high} AXL^{low} (501Mel) or the dedifferentiated MITF^{low} AXL^{high} (1205Lu) phenotypes. Consistently, LN-F contractility was inhibited by CM of 501Mel cells silenced for MITF expression by siRNA and pushed toward a dedifferentiated phenotype with increased AXL expression, compared with control 501Mel cells (**Fig. 2C** and supplementary Fig. S2B). These results were further validated by atomic force microscopy (AFM) analysis of collagen gels remodeled by LN-F. Indeed, gels treated with 1205Lu CM were softer than those treated with 501Mel CM, with similar stiffness to those treated with Y-27632 (**Fig. 2D**). Interestingly, LN-F embedded in collagen gels recovered their spontaneous

contractility upon 1205Lu CM withdrawal, demonstrating that melanoma cell-induced inhibition of LN-F contraction was a reversible process (**Fig. 2E**).

During an immune challenge, FRC activation is associated with proliferation, up-regulation of markers of fibroblast activation such as PDPN, and disruption of the RHOA-ROCK-mediated actomyosin cytoskeleton contraction due to CLEC2 interaction with PDPN (18,19,42). Similarly, the 1205Lu CM stimulated LN-F proliferation and increased PDPN cell surface expression whereas 501Mel CM had no effect (**Fig. 2F-G**). qRT-PCR analysis showed that expression of several markers of fibroblast activation like *PDPN*, *FAP*, *CXCL12*, *LIF* and *TNC* was also up-regulated by 1205Lu CM while *S100A4* (FSP1) and *ACTA2* (α-SMA) levels were not affected (**Fig. 2H**). Mass spectrometry (MS) analysis also revealed that 1205Lu-activated LN-F secreted more extracellular matrix proteins (TNC, FN) and cytokines (IL-6), validating the functional activation of LN-F (**Fig. 2I**). These results indicate that the inhibition of FRC contractility by dedifferentiated melanoma CM is a functional response of activated LN-F, like the FRC behavior observed during immunization. Importantly, our observations suggest that factors secreted by dedifferentiated and melanocytic melanoma cells do not share the same abilities to reprogram LN-F.

The propensity of fibroblasts to contract a collagen gel is regulated by forces generated by the actomyosin cytoskeleton (25,26). We next examined by immunofluorescence the F-actin organization and phosphorylation of the ROCK substrate MLC2 in LN-F treated with 501Mel CM or 1205Lu CM. The ROCK inhibitor Y-27632 was used as a control (**Fig. 3A-B**). We observed similar changes related to inhibition of actomyosin contraction (26) in LN-F treated with Y-27632 or 1205Lu CM, like decreased MLC2 S19 phosphorylation, less F-actin fibers, and the remodeling of the cell morphology from a stellate to a fusiform shape.

To identify the molecular pathways of LN-F contractility regulated by dedifferentiated melanoma CM, we performed microarray-based gene expression profiling on LN-F cultured in control conditions or exposed to 1205Lu CM (**Fig. 3C**). From the 25,000 most expressed LN-F genes, we selected differentially expressed genes (DEGs) with an absolute LogFC ≥ 0.5. We identified 1,113 DEGs up-regulated in 1205Lu CM-treated LN-F and 1,110 DEGs down-regulated, validating LN-F transcriptional reprogramming by dedifferentiated melanoma cells. Gene Set Enrichment Analysis

(GSEA) of the 1,110 down-regulated genes validated the inhibition of pathways related to actin cytoskeleton polymerization, RHOA GTPase activity and pointed towards the regulation of YAP and its co-transcription factor TEAD2 in 1205Lu-reprogrammed LN-F (**Fig. 3D** and Supplementary Fig. S3). GSEA plots also revealed that 1205Lu-treated LN-F converted from a myofibroblastic CAF signature to an inflammatory CAF signature (**Fig. 3E).**

Suppression of LN-F contractility by factors secreted by dedifferentiated melanoma cells is associated with impaired YAP activity.

To validate the inhibition of the YAP pathway identified by GSEA (**Fig. 3D** and **4A**), we investigated the effect of melanocytic and dedifferentiated melanoma cell CM on YAP nuclear localization and activation. Because YAP is sensitive to the cell microenvironment stiffness (27), its modulation by melanoma CM was investigated on hydrogels recapitulating the range of stiffness of LN-F-remodeled collagen gels (0.25 to 2.5 kPa) (**Fig. 2E**). In agreement with the inhibition of LN-F contractility induced by dedifferentiated melanoma cues, immunofluorescence analysis on 2.8 kPa hydrogels revealed that LN-F incubated with CM from dedifferentiated 1205Lu, WM793 or WM2032 cells exhibit an elongated shape, with more cytosolic YAP compared with control LN-F (**Fig. 4B**-**D**). In contrast, CM of 501Mel or SK-MEL-28 melanocytic cells did not induce any significant changes. Consistently, the expression of YAP target genes *CYR61, CTGF* and *SDPR* was decreased in LN-F treated with 1205Lu CM (**Fig. 4E**), as was the expression of genes regulated by the YAP co-transcription factor TEAD2 (**Fig. 4F**). Although less pronounced, similar results were obtained on 0.2 kPa hydrogels (**Fig. 4G-I**).

To address the contribution of YAP in LN-F contractility, YAP expression was silenced using a siRNA approach (**Fig. 4J**). The spontaneous LN-F-mediated collagen gel remodeling was suppressed by YAP knockdown, revealing that YAP is not only a marker of cell contraction, but actively controlled LN-F contractility. However, YAP depletion had no effect on LN-F proliferation (Supplementary Fig. S4A). Together, our data suggest that relaxation of the FRC actomyosin network induced by factors

secreted by dedifferentiated melanoma cells is associated with inhibition of YAP-TEAD2 transcriptional activity.

The JAK1-STAT3 pathway is inhibited by secreted factors from dedifferentiated melanoma cells and is involved in basal LN-F contraction.

Next, we sought to determine signaling pathways linking actomyosin cytoskeleton relaxation and YAP inhibition induced by melanoma secreted factors in LN-F. Previous studies demonstrated that actomyosin contraction of FRC was driven by the interaction of PDPN with proteins from the ERM family (21,22). Binding of PDPN to its ligand CLEC2 dismantled the PDPN-ERM interaction and inhibited ERM phosphorylation and PDPN-driven actomyosin contraction (18,19). However, our data excluded the possible contribution of the CLEC2-PDPN-ERM pathway in melanoma-induced LN-F relaxation. Indeed, CLEC2 was not detected in 1205Lu cells and ERM phosphorylation was not affected in 1205Lu CM-treated LN-F (**Fig. 5A**). In agreement with LN-F activation (**Fig. 2G**) and the concomitant inhibition of F-actin stress fiber formation observed in presence of 1205Lu CM (**Fig. 3A-B**), 1205Lu CM increased PDPN expression, and reduced α-SMA protein levels compared with 501Mel CM treatment or control LN-F.

Because TGF-β and IL-6 family cytokines are known to regulate ROCK-mediated actomyosin contraction in myofibroblasts and CAF (24,28,29), we next investigated if the TGF-βR1-SMAD and GP130-JAK-STAT pathways were also involved in LN-F contractility. The JAK1/2 inhibitor Ruxolitinib strongly inhibited the spontaneous contraction of LN-F isolated from 4 different donors while the TGF-βR1 inhibitor SB431542 had no effect (**Fig. 5B**). However, Ruxolitinib, SB431542 or Y-27632 had no effect on LN-F proliferation (Supplementary Fig. S4B). Importantly, immunoblot analysis revealed that Ruxolitinib inhibited both STAT3 and MLC2 phosphorylation, linking the JAK-STAT pathway to actomyosin contraction in LN-F (**Fig. 5C**). These results demonstrated that, beyond the CLEC2-PDPN-ERM pathway, LN-F contractility could also be controlled by the JAK-STAT pathway, but not by the TGF-βR1-SMAD pathway. Indeed, although STAT3 phosphorylation was increased early by 1205Lu CM, probably because of the high level of cytokines secreted by 1205Lu cells compared with 501Mel cells (36), it was maintained inhibited over the following days

(**Fig. 5D**). Sustained inhibition of STAT3 phosphorylation was also observed after 96h treatment with CM from the dedifferentiated WM2032 cell line or the short-term MM099 cells, but not after treatment with CM from the melanocytic short-term MM074 cells (**Fig. 5E**). The JAK-STAT3 pathway was thus specifically and consistently inhibited by factors secreted by dedifferentiated melanoma cells. Furthermore, both 1205Lu CM and Ruxolitinib inhibited RHOA activity in LN-F, suggesting that suppression of actomyosin contraction induced by 1205Lu CM was mediated through RHOA inhibition by the JAK-STAT pathway (**Fig. 5F**). Next, we identified JAK1 as the main JAK involved in LN-F contraction by showing that siRNA depletion of JAK1 (siJAK1), but not JAK2, inhibited LN-F-mediated collagen gel contraction, (**Fig. 5G**). Then, we validated that STAT3 depletion by siRNA inhibited LN-F collagen gel contraction, suggesting that JAK1 controlled LN-F contractility through STAT3 (**Fig. 5H**). JAK1 or STAT3 siRNAs had no effect on LN-F proliferation (Supplementary Fig. S4A). GSEA analysis of the 2,223 most regulated transcripts from the microarray revealed that several transcripts strongly up-regulated in 1205Lu CM-treated LN-F were indeed related to the negative regulation of the JAK-STAT pathway, such as *MIR146A*, *SOCS* (Suppressor Of Cytokine Signaling) family members and several phosphatases (**Fig. 5I**). Together, our results highlight the contribution of the JAK1-STAT3 pathway in the basal LN-F contraction and its inhibition by melanoma dedifferentiated cells.

The JAK1-STAT3 pathway controls YAP activity and the actin cytoskeleton polymerization.

We next questioned whether JAK1-STAT3 inhibition impacted on YAP function and actomyosin cytoskeleton remodeling in LN-F. JAK1 silencing by siRNA (siJAK1) induced YAP cytosolic relocation and inhibited the formation of actin filaments (**Fig. 5J-L**). Interestingly, similar modifications were observed after STAT3 depletion (siSTAT3), suggesting that JAK1 effects on YAP and actomyosin were mediated by STAT3. Accordingly, expression of the YAP target genes *CTGF* and *CYR61* was also inhibited after STAT3 silencing (**Fig. 5M**). Similar findings were observed with Ruxolitinib treatment, suggesting that the JAK1-STAT3 pathway is essential for maintaining nuclear YAP and actomyosin network tension (Supplementary Fig. S4C-F). After deciphering the signaling pathway modulated by dedifferentiated melanoma

cells to inhibit LN-F contraction, we turned our attention towards the pre-metastatic reprogramming of LN-F contractile properties *in vivo*.

Factors secreted by dedifferentiated melanoma cells inhibit murine LN-F contractility *in vivo* and decrease LN stiffness.

The pre-metastatic modulation of LN-F contractile properties was analyzed in two mouse models by tracking the cellular localization of YAP in LN-F of draining LN. On the one hand, CM of dedifferentiated 1205Lu cells and melanocytic 501Mel cells were respectively injected into each ear of nude mice (**Fig. 6A**). In this pre-metastatic model, CM from dedifferentiated 1205Lu cells induced cytosolic translocation of YAP in LN-F compared with CM from melanocytic 501Mel cells (**Fig. 6B-C**). On the other hand, CM of dedifferentiated murine melanoma cells YUMM1.7 and control medium were respectively injected into each ear of syngeneic C57Bl/6j mice (**Fig. 6D**). Analysis of *Mitf* and *Axl* expression by YUMM1.7 cells is shown in supplementary Fig. S5. In this syngeneic pre-metastatic model, CM from dedifferentiated YUMM1.7 melanoma cells induced cytosolic translocation of YAP in LN-F compared with control LN-F (**Fig. 6E-F**). In addition, YUMM1.7 CM induced swelling of the draining LN compared with the contralateral LN, and AFM analysis revealed that YUMM1.7 CM-draining LN were softer than control LN (**Fig. 6G**). These findings suggest that YAP-dependent inhibition of LN-F contractility is accompanied by changes in LN biomechanical properties.

Cytokines IL-1α and IL-1β secreted by dedifferentiated melanoma cells inhibit LN-F contractility.

The next step was to identify the nature of the tumor cues inhibiting LN-F contractility. The CM contains all factors secreted by melanoma cells, including soluble proteins and lipids and extracellular vesicles (EVs) such as exosomes. Although EVs are known to promote LN niche formation and distal metastatic tumor growth (12), we identified that LN-F contractility was not modulated by melanoma EVs but rather by soluble proteins (Supplementary Fig. S6A-C). We thus focused on proteins over-secreted by 1205Lu cells compared to 501Mel cells, as previously identified by MS and antibody

array analysis (35,36) (**Fig. 7A**). Candidate factors tested in gel contraction assays were restricted to secreted proteins present in the signature of dedifferentiated melanoma cells (8) (supplementary Fig. S6D), and found overexpressed by qRT-PCR in dedifferentiated cell lines 1205Lu, WM793, WM2032 compared to melanocytic cell lines 501Mel, MeWo, SK-MEL-28 (supplementary Fig. S6E). Following this strategy, we identified that IL-1α and IL-1β effectively inhibited LN-F contractility (**Fig. 7B**), whereas IL-6 or IL-8 had no effect (supplementary Fig. S6F). Both inflammatory cytokines bind to the IL1R1 receptor that is highly expressed by LN-F (43). ELISA analysis of melanoma CM confirmed that IL-1α and IL-1β were more secreted by dedifferentiated cells than by melanocytic cells (**Fig. 7C**) and that the ability of melanoma cells to inhibit LN-F contractility was strongly correlated with the amount of IL-1α and IL-1β secreted (**Fig. 7D**). As CM from dedifferentiated melanoma cells, IL-1α or IL-1β inhibited STAT3 phosphorylation in LN-F (**Fig. 7E**). Furthermore, *IL1A* and *IL1B* expressions were significantly inversely associated with *MITF* expression in melanoma patients (Skin cutaneous melanoma TCGA dataset) (**Fig. 7F**). Our results thus show that IL-1α and IL-1β cytokines secreted by dedifferentiated melanoma cells inhibit LN-F contractility.

LN-F reprogrammed by dedifferentiated melanoma cells promote melanoma cell invasiveness.

To understand the role played by inhibition of LN-F contractility by dedifferentiated melanoma cells in metastatic progression, melanoma cells were first cultured on confluent monolayers of contracted or relaxed LN-F. The proliferation and 2D migration of 1205Lu fluorescent cells (1205Lu Red), monitored by real-time microscopy, were not affected by reprograming of LN-F with 1205Lu CM, IL-1β or Y-27632 (supplementary Fig. S7A-B), indicating that LN-F relaxation did not modulate cancer cell proliferation or migration. Next, 3D invasion of 1205Lu Red cells into LN-F remodeled collagen gels was analyzed by confocal microscopy (**Fig. 8A-B**). Whereas 40% to 60% of the cancer cells browsed 30 µm in gels remodeled by relaxed LN-F treated with 1205Lu CM, IL-1β or Y-27632, less than 20% did so in gels remodeled by contracted LN-F treated with control medium or 501Mel CM (**Fig. 8C**). In parallel, the z-distance covered by the 5% more invasive 1205Lu Red cells was increased from 40-

70 µm to 100-130 µm between collagen gels remodeled by relaxed LN-F compared to resting LN-F (**Fig. 8D**). These results indicate that the inhibition of LN-F contractility driven by dedifferentiated melanoma cells strongly enhances 3D cancer cell invasion.

Discussion

Our study provides evidence that human FRC are contractile cells like murine FRC (18-20). Quiescent FRC display a myofibroblast-like phenotype along with high expression of PDPN, FAP and α-SMA and thus share many properties with CAF. These CAF hallmarks suggest that FRC could play a tumor supportive role in the LN metastatic microenvironment. Indeed, PDPN was identified as a CAF marker in a variety of malignancies and is associated with metastasis and poor prognosis (44,45). PDPN expression on CAF favors force-mediated matrix remodeling through the activation of the RHO-ROCK pathway and promotes cancer cell invasion (45). In breast cancer patients, metastatic LN are enriched in a CAF subpopulation inducing cancer cell invasion and exhibiting similar markers ($PDPN^{high}$, FAP^{high}, $\alpha\text{-}SMA^{high}$, $PDGFR\text{-}\beta^{high}$) to FRC (46), suggesting that LN CAF mostly originated from resident FRC.

Focusing on the signaling pathway(s) driving FRC actomyosin contractility, we provide evidence that the spontaneous contractility of quiescent FRC relies on a basal level of YAP and JAK1-STAT3 activation, and not only on the PDPN-ERM pathway as previously identified in murine FRC. YAP activation is known to reflect the actomyosin contractile state of FRC (19) and CAF (26), and to regulate FRC differentiation during LN development (47). We show here that YAP is not only a marker but also controls actomyosin contractility of differentiated human FRC. YAP and the RHO-ROCK pathway are intimately linked, regulating each other, and controlling the actomyosin cytoskeleton plasticity (26,27). We also disclose that inhibition of JAK1 or STAT3 reduces FRC contractility and leads to inhibition of RHOA and YAP. Interestingly, our MS analysis suggests that basal JAK1-STAT3 signaling in resting human FRC could be due to autocrine secretion of IL-6 (**Fig. 2I**). Previous studies have shown that JAK1-STAT3 signaling increases ROCK-mediated actomyosin contractility in CAF, and that ROCK signaling induces STAT3 phosphorylation and transcriptional responses. Thus,

JAK1-STAT3 and RHO-ROCK are interdependent and cross-regulate each other (29). Collectively, our results support the notion that the RHO-ROCK-driven contractility of human FRC is not only controlled by the PDPN-ERM pathway, but also by signaling pathways shared with CAF.

Tumor cells secrete growth factors and inflammatory factors, such as TGF-β or IL-6 family cytokines, which trigger fibroblast activation and CAF transformation, both of which are associated with increased actomyosin contractility. Strikingly, dedifferentiated melanoma cells, but not melanocytic melanoma cells, secrete factors drastically suppressing force-driven collagen gel remodeling by FRC. Factors secreted by dedifferentiated melanoma cells inhibit JAK1-STAT3 signaling, which decreases RHO-ROCK-MLC2 signaling and YAP activity. During an immune challenge, FRC relaxation is associated with FRC activation (18,19). Similarly, FRC stimulated with CM from dedifferentiated melanoma cells show an activated phenotype: they proliferate more, up-regulate markers of activation, and increase the secretion of extracellular matrix proteins and cytokines. Interestingly, both BRAF-mutated (1205Lu, WM793, MM099) and NRAS-mutated (WM2032, SBcl2) dedifferentiated melanoma cells were able to inhibit FRC contractility. The question remains whether tumor-derived factors from other cancers that spread to the LN, such as breast cancer, can exert a similar task on FRC.

Culture of FRC with factors secreted by dedifferentiated melanoma cells strikingly phenocopies the prevention of PDPN signaling by the provision of CLEC2, antibody blockade or genetic deficiency (18,19). It induces similar morphological changes with an elongated cell shape, decreased stress fibers, less YAP nuclear activation, but also increased proliferation and PDPN expression. So, while we have excluded the modulation of ERM phosphorylation by melanoma CM, the implication of PDPN in the inhibition of FRC contractility mediated by melanoma CM is still an open question. Interestingly, PDPN can also activate the FRC actomyosin machinery independently of its binding to ERM proteins, by engaging a neighboring transmembrane protein (19). This unknown transmembrane protein may drive JAK1 signaling and binding to its ligand secreted by dedifferentiated melanoma cells could dissociate such interaction. In light of our results, the IL-1 receptor IL1R1 might be an interesting candidate as it is highly expressed in FRC (43). Alternatively, JAK1 may directly bind to the cytoplasmic

tail of PDPN through its N-terminal FERM domain (48). PDPN controls a wide range of physiological effects, such as contractility, migration, proliferation, or differentiation. Multiple molecular mechanisms of PDPN regulation are therefore likely in various cell types (45).

It is established that factors secreted by melanoma cells, including TGF-β, growth factors, or proinflammatory molecules promote tumorigenesis (49) and LN metastasis (13). Melanoma EVs have been particularly described as potent inducers of LN pre-metastatic niches (12), but did not modulate FRC contractility in our experimental setting. Analyses of factors preferentially secreted by dedifferentiated melanoma cells (35,36) and inhibiting LN-F contractility pointed towards the IL-1 inflammatory cytokine, although the participation of other tumoral factors cannot be excluded. IL-1 plays an important role in tumor progression and metastasis (50) and is detected at high levels in the serum of melanoma patients (51). Interestingly, FRC express high levels of IL1R1 and respond rapidly to systemic IL-1β stimulation *in vivo* (43). Furthermore, IL-1 inhibits the contractility of lung fibroblasts (52-54). The link between IL-1 and inhibition of the JAK1-STAT3 pathway needs further investigation, but it may involve activation of the p38 MAPK, as in synovial fibroblasts (55).

LN are less stiff and more deformable following antibody blockade of PDPN and FRC contractility (19). Although other factors, such as lymph transport and immune cell recruitment, participate in modulating the biomechanical properties of the pre-metastatic LN (15,16,31), our results *in vivo* validate that FRC contractility impacts LN stiffness and show that it is controlled by factors secreted by dedifferentiated melanoma cells. Melanoma-induced stromal reprogramming in the tumor draining LN has been analyzed in other studies using the murine cell line B16.F10 (16,31). B16.F10 cells do not harbor classic human melanoma mutations (BRAF, NRAS or NF1) and are known to express high levels of MITF despite their metastatic potential. In contrast to our results with melanocytic $MITF^{high}$ melanoma cells, these studies reported the enhanced capacity of FRC treated with B16.F10 CM to contract collagen gels, the increased RHO signaling in murine FRC isolated from B16.F10-draining LN and increased stiffness and intranodal pressure of B16.F10-draining LN. The reason behind this discrepancy remains unclear but suggests that B16.F10 cells may control FRC contractility differently from human melanocytic melanoma cells. These results

underline that metastatic disease development is a highly complex process fueled by intra-tumoral heterogeneity and mutational background.

Plasticity of melanoma cells is considered a key driver in the development of the disease and cellular phenotypes drive individual steps of melanoma progression (2-5). The phenotype of dedifferentiated cells is associated with increased invasive and metastatic capabilities. Our findings further suggest that the dedifferentiated state, in contrast to the melanocytic state, allows melanoma cells to reprogram the fibroblastic stroma of the LN prior to metastatic dissemination, and that this contributes to LN tumor invasion. FRC contractile phenotype regulates LN swelling and tunes LN immunity (18,19). Furthermore, microenvironment clues such as tissue stiffness regulates the properties of tumor cells. Our data therefore suggest that significant changes in LN stiffness and FRC network microstructure could modulate the metastatic capabilities of tumor cells, but also the anti-tumor immune response. Our data show that relaxation of the FRC three-dimensional network in collagen gels increases the invasive capabilities of melanoma cells. Thus, reprogramming of LN biomechanical and immune properties by loss of FRC contractility could be essential for survival and development of metastatic cells in the LN niche.

In conclusion, we identified that factors secreted by dedifferentiated melanoma cells, such as IL-1, reprogram the functions of FRC from the tumor-draining LN and deciphered the underlying signaling pathways involved in human FRC cytoskeleton relaxation. Our work illustrates that FRC activation and actomyosin relaxation in the LN might be a prognostic marker of melanoma invasive potential, suggesting that the microarchitecture of the FRC reticular network and PDPN expression could be examined in tumor-draining LN at diagnosis. Our data also reinforce the rational for clinical trials combining anti-IL1 strategies with checkpoint blockade immunotherapy (50). Blocking remote communication between dedifferentiated melanoma cells and the FRC may inhibit the formation of a permissive biomechanical and immunological LN niche, thereby impinging on lymphatic metastasis.

Acknowledgments

This work was funded by Institut National de la Santé et de la Recherche Médicale (Inserm), Université Côte d'Azur, Canceropôle Provence Alpes Côte d'Azur (Emergence grant to V. Prod'homme), Fondation ARC (Projet Fondation ARC to V. Prod'homme), Ligue Contre le Cancer (Equipe labellisée to S. Tartare-Deckert) and Institut National du Cancer (INCA_12673 to S. Tartare-Deckert). Funding from Agence Nationale de la Recherche (ANR-18-CE14-0019-01 to M. Deckert), ITMO Cancer Aviesan within the framework of the Cancer Plan and the French Government through the ''Investments for the Future'' Labex SIGNALIFE (ANR-11-LABX- 0028-01) are also acknowledged. I. Berestjuk is a recipient of a doctoral fellowship from Ligue Contre le Cancer and S. Diazzi is a recipient of a doctoral fellowship from Fondation pour la Recherche Médicale (FRM). We thank J.-C. Marine and G. Ghanem for short-term cultures of melanoma cells, M. Bosenberg for YUMM1.7 cells and the Microscopie Imagerie Côte d'Azur (MICA) platform supported by the GIS IBiSA, the Conseil Départemental 06 and the Région Provence-Alpes-Côte d'Azur. We also acknowledge the HistoC3M histology facility funded by the Canceropôle Provence-Alpes-Côte d'Azur, and the AFM core facility supported by the Fondation ARC, the GIS IBiSA and the Conseil Général 06 de la Région Provence-Alpes-Côte d'Azur.

References

1. Cancer Genome Atlas N. Genomic Classification of Cutaneous Melanoma. Cell **2015**;161:1681-96
2. Arozarena I, Wellbrock C. Phenotype plasticity as enabler of melanoma progression and therapy resistance. Nat Rev Cancer **2019**;19:377-91
3. Hoek KS, Eichhoff OM, Schlegel NC, Dobbeling U, Kobert N, Schaerer L*, et al.* In vivo switching of human melanoma cells between proliferative and invasive states. Cancer Res **2008**;68:650-6
4. Rambow F, Rogiers A, Marin-Bejar O, Aibar S, Femel J, Dewaele M*, et al.* Toward Minimal Residual Disease-Directed Therapy in Melanoma. Cell **2018**;174:843-55 e19
5. Wouters J, Kalender-Atak Z, Minnoye L, Spanier KI, De Waegeneer M, Bravo Gonzalez-Blas C*, et al.* Robust gene expression programs underlie recurrent cell states and phenotype switching in melanoma. Nat Cell Biol **2020**;22:986-98
6. Girard CA, Lecacheur M, Ben Jouira R, Berestjuk I, Diazzi S, Prod'homme V*, et al.* A Feed-Forward Mechanosignaling Loop Confers Resistance to Therapies Targeting the MAPK Pathway in BRAF-Mutant Melanoma. Cancer Res **2020**;80:1927-41

7. Shaffer SM, Dunagin MC, Torborg SR, Torre EA, Emert B, Krepler C*, et al.* Rare cell variability and drug-induced reprogramming as a mode of cancer drug resistance. Nature **2017**;546:431-5
8. Verfaillie A, Imrichova H, Atak ZK, Dewaele M, Rambow F, Hulselmans G*, et al.* Decoding the regulatory landscape of melanoma reveals TEADS as regulators of the invasive cell state. Nat Commun **2015**;6:6683
9. Brown M, Assen FP, Leithner A, Abe J, Schachner H, Asfour G*, et al.* Lymph node blood vessels provide exit routes for metastatic tumor cell dissemination in mice. Science **2018**;359:1408-11
10. Pereira ER, Kedrin D, Seano G, Gautier O, Meijer EFJ, Jones D*, et al.* Lymph node metastases can invade local blood vessels, exit the node, and colonize distant organs in mice. Science **2018**;359:1403-7
11. Ubellacker JM, Tasdogan A, Ramesh V, Shen B, Mitchell EC, Martin-Sandoval MS*, et al.* Lymph protects metastasizing melanoma cells from ferroptosis. Nature **2020**;585:113-8
12. Hood JL, San RS, Wickline SA. Exosomes released by melanoma cells prepare sentinel lymph nodes for tumor metastasis. Cancer Res **2011**;71:3792-801
13. Olmeda D, Cerezo-Wallis D, Riveiro-Falkenbach E, Pennacchi PC, Contreras-Alcalde M, Ibarz N*, et al.* Whole-body imaging of lymphovascular niches identifies pre-metastatic roles of midkine. Nature **2017**;546:676-80
14. Cochran AJ, Huang RR, Lee J, Itakura E, Leong SP, Essner R. Tumour-induced immune modulation of sentinel lymph nodes. Nat Rev Immunol **2006**;6:659-70
15. Commerford CD, Dieterich LC, He Y, Hell T, Montoya-Zegarra JA, Noerrelykke SF*, et al.* Mechanisms of Tumor-Induced Lymphovascular Niche Formation in Draining Lymph Nodes. Cell Rep **2018**;25:3554-63 e4
16. Riedel A, Shorthouse D, Haas L, Hall BA, Shields J. Tumor-induced stromal reprogramming drives lymph node transformation. Nat Immunol **2016**;17:1118-27
17. Fletcher AL, Acton SE, Knoblich K. Lymph node fibroblastic reticular cells in health and disease. Nat Rev Immunol **2015**;15:350-61
18. Acton SE, Farrugia AJ, Astarita JL, Mourao-Sa D, Jenkins RP, Nye E*, et al.* Dendritic cells control fibroblastic reticular network tension and lymph node expansion. Nature **2014**;514:498-502
19. Astarita JL, Cremasco V, Fu J, Darnell MC, Peck JR, Nieves-Bonilla JM*, et al.* The CLEC-2-podoplanin axis controls the contractility of fibroblastic reticular cells and lymph node microarchitecture. Nat Immunol **2015**;16:75-84
20. Malhotra D, Fletcher AL, Astarita J, Lukacs-Kornek V, Tayalia P, Gonzalez SF*, et al.* Transcriptional profiling of stroma from inflamed and resting lymph nodes defines immunological hallmarks. Nat Immunol **2012**;13:499-510
21. Martin-Villar E, Megias D, Castel S, Yurrita MM, Vilaro S, Quintanilla M. Podoplanin binds ERM proteins to activate RhoA and promote epithelial-mesenchymal transition. J Cell Sci **2006**;119:4541-53
22. Wicki A, Lehembre F, Wick N, Hantusch B, Kerjaschki D, Christofori G. Tumor invasion in the absence of epithelial-mesenchymal transition: podoplanin-mediated remodeling of the actin cytoskeleton. Cancer Cell **2006**;9:261-72
23. Diazzi S, Tartare-Deckert S, Deckert M. Bad Neighborhood: Fibrotic Stroma as a New Player in Melanoma Resistance to Targeted Therapies. Cancers (Basel) **2020**;12

24. Kalluri R. The biology and function of fibroblasts in cancer. Nat Rev Cancer **2016**;16:582-98
25. Gaggioli C, Hooper S, Hidalgo-Carcedo C, Grosse R, Marshall JF, Harrington K*, et al.* Fibroblast-led collective invasion of carcinoma cells with differing roles for RhoGTPases in leading and following cells. Nat Cell Biol **2007**;9:1392-400
26. Calvo F, Ege N, Grande-Garcia A, Hooper S, Jenkins RP, Chaudhry SI*, et al.* Mechanotransduction and YAP-dependent matrix remodelling is required for the generation and maintenance of cancer-associated fibroblasts. Nat Cell Biol **2013**;15:637-46
27. Dupont S, Morsut L, Aragona M, Enzo E, Giulitti S, Cordenonsi M*, et al.* Role of YAP/TAZ in mechanotransduction. Nature **2011**;474:179-83
28. Albrengues J, Bourget I, Pons C, Butet V, Hofman P, Tartare-Deckert S*, et al.* LIF mediates proinvasive activation of stromal fibroblasts in cancer. Cell Rep **2014**;7:1664-78
29. Sanz-Moreno V, Gaggioli C, Yeo M, Albrengues J, Wallberg F, Viros A*, et al.* ROCK and JAK1 signaling cooperate to control actomyosin contractility in tumor cells and stroma. Cancer Cell **2011**;20:229-45
30. Albrengues J, Bertero T, Grasset E, Bonan S, Maiel M, Bourget I*, et al.* Epigenetic switch drives the conversion of fibroblasts into proinvasive cancer-associated fibroblasts. Nat Commun **2015**;6:10204
31. Rohner NA, McClain J, Tuell SL, Warner A, Smith B, Yun Y*, et al.* Lymph node biophysical remodeling is associated with melanoma lymphatic drainage. FASEB J **2015**;29:4512-22
32. Robert G, Gaggioli C, Bailet O, Chavey C, Abbe P, Aberdam E*, et al.* SPARC represses E-cadherin and induces mesenchymal transition during melanoma development. Cancer Res **2006**;66:7516-23
33. Berestjuk I, Lecacheur M, Carminati A, Diazzi S, Rovera C, Prod'homme V*, et al.* Targeting Discoidin Domain Receptors DDR1 and DDR2 overcomes matrix-mediated tumor cell adaptation and tolerance to BRAF-targeted therapy in melanoma. EMBO Mol Med **2021**:e11814
34. Didier R, Mallavialle A, Ben Jouira R, Domdom MA, Tichet M, Auberger P*, et al.* Targeting the Proteasome-Associated Deubiquitinating Enzyme USP14 Impairs Melanoma Cell Survival and Overcomes Resistance to MAPK-Targeting Therapies. Mol Cancer Ther **2018**;17:1416-29
35. Rathore M, Girard C, Ohanna M, Tichet M, Ben Jouira R, Garcia E*, et al.* Cancer cell-derived long pentraxin 3 (PTX3) promotes melanoma migration through a toll-like receptor 4 (TLR4)/NF-kappaB signaling pathway. Oncogene **2019**;38:5873-89
36. Tichet M, Prod'Homme V, Fenouille N, Ambrosetti D, Mallavialle A, Cerezo M*, et al.* Tumour-derived SPARC drives vascular permeability and extravasation through endothelial VCAM1 signalling to promote metastasis. Nature Communications **2015**;6
37. Dankort D, Curley DP, Cartlidge RA, Nelson B, Karnezis AN, Damsky WE, Jr.*, et al.* Braf(V600E) cooperates with Pten loss to induce metastatic melanoma. Nat Genet **2009**;41:544-52
38. Lino Cardenas CL, Henaoui IS, Courcot E, Roderburg C, Cauffiez C, Aubert S*, et al.* miR-199a-5p Is upregulated during fibrogenic response to tissue injury and mediates TGFbeta-induced lung fibroblast activation by targeting caveolin-1. PLoS Genet **2013**;9:e1003291

39. Tse JR, Engler AJ. Preparation of hydrogel substrates with tunable mechanical properties. Curr Protoc Cell Biol **2010**;Chapter 10:Unit 10 6
40. Rodda LB, Lu E, Bennett ML, Sokol CL, Wang X, Luther SA*, et al.* Single-Cell RNA Sequencing of Lymph Node Stromal Cells Reveals Niche-Associated Heterogeneity. Immunity **2018**;48:1014-28 e6
41. Hinz B, Celetta G, Tomasek JJ, Gabbiani G, Chaponnier C. Alpha-smooth muscle actin expression upregulates fibroblast contractile activity. Mol Biol Cell **2001**;12:2730-41
42. Yang CY, Vogt TK, Favre S, Scarpellino L, Huang HY, Tacchini-Cottier F*, et al.* Trapping of naive lymphocytes triggers rapid growth and remodeling of the fibroblast network in reactive murine lymph nodes. Proc Natl Acad Sci U S A **2014**;111:E109-18
43. Song A, Zhu L, Gorantla G, Berdysz O, Amici SA, Guerau-de-Arellano M*, et al.* Salient type 1 interleukin 1 receptor expression in peripheral non-immune cells. Sci Rep **2018**;8:723
44. Kan S, Konishi E, Arita T, Ikemoto C, Takenaka H, Yanagisawa A*, et al.* Podoplanin expression in cancer-associated fibroblasts predicts aggressive behavior in melanoma. J Cutan Pathol **2014**;41:561-7
45. Quintanilla M, Montero-Montero L, Renart J, Martin-Villar E. Podoplanin in Inflammation and Cancer. Int J Mol Sci **2019**;20
46. Pelon F, Bourachot B, Kieffer Y, Magagna I, Mermet-Meillon F, Bonnet I*, et al.* Cancer-associated fibroblast heterogeneity in axillary lymph nodes drives metastases in breast cancer through complementary mechanisms. Nat Commun **2020**;11:404
47. Choi SY, Bae H, Jeong SH, Park I, Cho H, Hong SP*, et al.* YAP/TAZ direct commitment and maturation of lymph node fibroblastic reticular cells. Nat Commun **2020**;11:519
48. Haan S, Margue C, Engrand A, Rolvering C, Schmitz-Van de Leur H, Heinrich PC*, et al.* Dual role of the Jak1 FERM and kinase domains in cytokine receptor binding and in stimulation-dependent Jak activation. J Immunol **2008**;180:998-1007
49. Melnikova VO, Bar-Eli M. Inflammation and melanoma metastasis. Pigment Cell Melanoma Res **2009**;22:257-67
50. Garlanda C, Mantovani A. Interleukin-1 in tumor progression, therapy, and prevention. Cancer Cell **2021**;39:1023-7
51. Yurkovetsky ZR, Kirkwood JM, Edington HD, Marrangoni AM, Velikokhatnaya L, Winans MT*, et al.* Multiplex analysis of serum cytokines in melanoma patients treated with interferon-alpha2b. Clin Cancer Res **2007**;13:2422-8
52. Gabasa M, Arshakyan M, Llorente A, Chulia-Peris L, Pavelescu I, Xaubet A*, et al.* Interleukin-1beta Modulation of the Mechanobiology of Primary Human Pulmonary Fibroblasts: Potential Implications in Lung Repair. Int J Mol Sci **2020**;21
53. Osei ET, L BM-G, Hsieh A, Warner SM, Al-Fouadi M, Wang M*, et al.* Epithelial-interleukin-1 inhibits collagen formation by airway fibroblasts: Implications for asthma. Sci Rep **2020**;10:8721
54. Zhang HY, Gharaee-Kermani M, Phan SH. Regulation of lung fibroblast alpha-smooth muscle actin expression, contractile phenotype, and apoptosis by IL-1beta. J Immunol **1997**;158:1392-9
55. Deon D, Ahmed S, Tai K, Scaletta N, Herrero C, Lee IH*, et al.* Cross-talk between IL-1 and IL-6 signaling pathways in rheumatoid arthritis synovial fibroblasts. J Immunol **2001**;167:5395-403

Figure legends

Figure 1. LN-F display a CAF-like phenotype associated with spontaneous contraction and expression of CAF markers.

(A) Pictures of collagen gels containing LN-F from 4 donors (#1 to #4) treated with control medium (Ctrl) or the ROCK inhibitor Y-27632 (10 µM) for 8 days and quantification of the LN-F-mediated collagen gel contraction (in quadruplicate; mean +/- SEM; p-Val (****)<0.0001)). (B) Collagen gel contraction induced by LN-F, skin-F or CAFs isolated from skin melanomas or LN melanomas and treated with Ctrl medium, TGF-β (2 ng/ml) or Y-27632 (10 µM) for 7 days (n = 2 to 7 for each cell type, in triplicate; mean +/- SEM; p-Val (*)<0.05, (***)<0.001, (****)<0.0001). (C) Fluorescence pictures showing F-actin fibers, cell nuclei (Hoechst) and YAP localization in Skin-F and LN-F grown for 4 days in control medium or with TGF-β (2 ng/ml) (Scale bar = 100 µm). (D) Quantification of F-actin integrated density (n = 19 cells; median +/- quartiles) and YAP localization (n = 22 cells; median +/- quartiles); p-Val (**)<0.01, (****)<0.0001). (E) Quantification by qRT-PCR of the fold expression of CAF markers in LN-F and Skin-F (n = 2, in duplicate; mean +/- SEM; p-Val (*)<0.05, (***)<0.001, (****)<0.0001). (F) Immunoblotting of CAF markers (FN, PDGFRβ, FAP and α-SMA) in Skin-F and LN-F cultured for 4 days in control medium or treated by TGF-β (2 ng/ml). HSP60 is used as a loading control. Fragments of the same original image are cropped to re-order lanes or to remove irrelevant lanes.

Figure 2. Factors secreted by MITF^{low} AXL^{high} dedifferentiated melanoma cells inhibit LN-F contractility and induce LN-F proliferation and activation.

(A) Representative pictures (left) and quantification (right) of LN-F-mediated contraction of collagen gels after 7 days culture with control medium (Ctrl) or CM from dedifferentiated MITF^{low} AXL^{high} or melanocytic MITF^{high} AXL^{low} melanoma cell lines or short-term patient melanoma cells (n = 3, in triplicate; mean +/- SEM; p-Val (**)<0.01, (****)<0.0001). (B) Spearman correlation analysis of MITF gene expression (Log) by melanoma cells versus the % of LN-F-mediated collagen gel contraction shown in (A). (C) Immunoblotting of MITF and HSP60 (loading control) 3 days after siRNA silencing

of MITF (siMITF) (left). LN-F-mediated contraction of collagen gels incubated with CM from 501Mel siMITF or 501Mel siCtrl (n = 3, in quadruplicate; mean +/- SEM; p-Val (*)<0.05) (right). (D) Quantification by atomic force microscopy of the collagen gel stiffness, expressed as Log_{10} of the apparent Young's (elastic) modulus distribution, following contraction by LN-F treated for 9 days with the ROCK inhibitor Y-27632 (10 µM), 501Mel CM or 1205Lu CM (n = 2, in duplicate; median +/- quartiles; p-Val (****)<0.0001). Median values are respectively 0.29 kPa, 1.68 kPa and 0.27 kPa. Representative collagen gels are shown above the violin plots. (E) Time-lapse analysis of LN-F-mediated collagen gel contraction (n = 2, in quadruplicate; mean +/- SEM). The 1205Lu CM is replaced by Ctrl medium after 2, 4 or 8 days. (F) Proliferation of LN-F incubated for 6 days with Ctrl medium, 501Mel CM or 1205Lu CM (n = 2, in triplicate; mean +/- SEM; p-Val (**)<0.01). (G) Representative flow cytometry analysis (left) and quantification (right) of PDPN surface expression on LN-F cultured for 5 days with 1205Lu CM (in red) or Ctrl medium (in blue). Staining with a control isotype mAb is shown in grey (n = 4, in duplicate). (H) qRT-PCR analysis of fibroblast activation markers expressed by LN-F cultured for 2 days with Ctrl medium, 501Mel CM or 1205Lu CM (n = 2, in duplicate; Mean +/- SEM; p-Val (*)<0.05, (**)<0.01, (***)<0.001). (I) Detection by mass spectrometry of TNC, FN and IL6 secreted by LN-F treated for 7 days with Ctrl medium or 1205Lu CM (n = 2, in triplicate; Mean +/- SEM; p-Val (**)<0.01, (***)<0.001).

Figure 3. Factors secreted by MITF^{low} AXL^{high} dedifferentiated melanoma cells inhibit actomyosin cytoskeleton contraction of LN-F.

(A) Fluorescence staining of F-actin fibers, MLC2 phosphorylation (P-MLC2) and cell nuclei (Hoechst) in LN-F grown for 7 days in control (Ctrl) medium or with CM from the dedifferentiated 1205Lu cell line or the melanocytic 501Mel cell line (Scale bar = 100 µm). A zoom on a single cell is shown for each condition (Scale bar = 20 µm). (B) Quantification of mean fluorescence intensities (MFI) of active pS19 MLC2 (P-MLC2), F-actin fibers and the cell shape index (n = 45 cells; median +/- quartiles; p-Val (*)<0.05, (***)<0.001, (****)<0.0001). (C) Microarray-based gene expression profiling in Ctrl and 1205Lu CM-treated LN-F. The 1,110 most down-regulated genes in 1205Lu-reprogrammed LN-F (with LogFC ≤ - 0.5) are surrounded and submitted to

Gene Set Enrichment Analysis (GSEA) in (D). (E) GSEA plot comparing the gene expression of Ctrl- and 1205Lu-educated LN-F with signatures from inflammatory CAFs and myofibroblastic CAFs.

Figure 4. The inhibition of LN-F contractility induced by dedifferentiated melanoma CM is associated with decreased YAP activity.

(A) Top genes down-regulated in 1205Lu CM-treated LN-F in the Cordenonsi YAP conserved Signature (LogFC ≤ - 0.5). (B) Immunofluorescence analysis of YAP and Hoechst localization in LN-F plated on 2.8 kPa hydrogels and treated 4 days with control (Ctrl) medium, proliferative or invasive melanoma CM (Scale bar = 50 µm). (C) Analysis of the cell shape index of LN-F plated on 2.8 kPa hydrogels and treated 4 days with ctrl medium, proliferative or invasive melanoma CM (n = 20 cells; median +/- quartiles; p-Val (*)<0.05, (**)<0.01). (D) Quantification of YAP nuclear and cytosolic localization in LN-F plated on 2.8 kPa hydrogels and treated 4 days with ctrl medium, proliferative or invasive melanoma CM (n = 32 cells; median +/- quartiles; p-Val (****)<0.0001). (E) Quantification by qRT-PCR of the expression of YAP target genes in LN-F plated on 2.8 kPa hydrogels and treated 4 days with 501Mel CM or 1205Lu CM (n = 2, in duplicate; mean +/- SEM; p-Val (***)<0.001, (****)<0.0001). (F) Top TEAD2 target genes down-regulated in 1205Lu CM-treated LN-F (LogFC ≤ - 0.5, pVal ≤ 0.05). (G) Immunofluorescence analysis of YAP and Hoechst localization in LN-F plated on 0.2 kPa hydrogels and treated 4 days with 501Mel CM or 1205Lu CM (Scale bar = 50 µM). (H) Quantification of YAP nuclear and cytosolic localization in LN-F plated on 0.2 kPa hydrogels and treated 4 days with 501Mel CM or 1205Lu CM (n = 15 cells, median +/- quartiles, p-Val (*)<0.05). (I) Quantification by qRT-PCR of the expression of YAP target genes by LN-F plated on 0.2 kPa hydrogels and treated 4 days with 501Mel CM or 1205Lu CM (n = 2 in duplicate, mean +/- SEM, p-Val (*)<0.05). (J) Immunoblotting of YAP and ERK2 (loading control) 3 days after the extinction of YAP expression by 2 siRNAs (siYAP#1 and siYAP#2) (left). Quantification of LN-F-mediated gel contraction after siRNA silencing of YAP (n = 3, in quadruplicate; mean +/- SEM; p-Val (**)<0.01, (****)<0.0001) (right). A control siRNA (siCtrl) is used as a control of transfection.

Figure 5. The JAK1-STAT3 pathway is inhibited by dedifferentiated melanoma CM and controls LN-F contraction.

(A) Immunoblotting of PDPN, P-ERM, ERM and α-SMA in LN-F cultured in control medium, 501Mel CM or 1205Lu CM for 10 min, 30 min, 1 h, 3 h, 24 h and 96 h. HSP60 is used as a loading control. Fragments of the same original image are cropped to re-order lanes or to remove irrelevant lanes. (B) Collagen gel contraction by LN-F treated by 10 µM of TGF-βR1 inhibitor (SB431542) or Ruxolitinib for 8 days (n = 3, in quadruplicate; mean +/- SEM; p-Val (****)<0.0001). These inhibitors were tested at the same time as the experiment shown in Figure 1A and have the same Ctrl wells. (C) Immunoblotting of P-STAT3, STAT3, P-MLC2 and MLC2 in LN-F treated 4 days by Ruxolitinib (10µM) or Y-27632 (10µM). HSP60 is used as a loading control. Fragments of the same original image are cropped to re-order lanes or to remove irrelevant lanes. (D) Immunoblotting of P-STAT3 and STAT3 in LN-F cultured in Ctrl medium, 501Mel CM or 1205Lu CM for 20 min, 2 h, 24 h and 96 h. HSP60 is used as a loading control. (E) Immunoblotting of P-STAT3 and STAT3 in LN-F cultured for 96 h in Ctrl medium or CM from short term isolated melanoma cells (MM074 and MM099) or melanoma cell lines (501Mel, 1205Lu, WM2032). HSP60 is used as a loading control. (F) RHOA activity measured by G-LISA assay in cell lysates of LN-F treated 4 days with 501Mel CM, 1205Lu CM or Ruxolitinib (10µM) (n = 3, in triplicate; mean +/- SEM; p-Val (*)<0.05, (**)<0.01). (G) qRT-PCR quantification of JAK1 and JAK2 silencing by siRNAs (siJAK1 and siJAK2) (n = 2, in duplicate) (left) and quantification of collagen gel contraction by LN-F transfected with siJAK1 or siJAK2 (n = 2, in triplicate; mean +/- SEM; p-Val (**)<0.01) (right). A ctrl siRNA (siCtrl) is used as a control of transfection. (H) Immunoblotting of STAT3 and Tubulin-α 2 days after the extinction of STAT3 expression by 2 siRNAs (siSTAT3#1 and siSTAT3#2) (left). Quantification of LN-F-mediated gel contraction after siRNA silencing of STAT3 (n = 2, in quadruplicate; mean +/- SEM; p-Val (****)<0.0001) (right). A control siRNA (siCtrl) is used as a control of transfection. (I) Differentially expressed genes between Ctrl and 1205Lu CM-treated LN-F identified in the GO negative regulation of receptor signaling pathway via STAT. (J) Immunofluorescence analysis of YAP, F-actin fibers and Hoechst in LN-F depleted from YAP (siYAP) or STAT3 (siSTAT3) expression by siRNA. The siCtrl siRNA is used

as a control of transfection (Scale bar = 100 µM). (K) Quantification of YAP localization (n = 50 cells; median +/- quartiles; p-Val (**)<0.01, (****)<0.0001). (L) Quantification of F-actin integrated density (n = 44 cells; median +/- quartiles; p-Val (*)<0.05, (**)<0.01). (M) qRT-PCR analysis of the expression of YAP target genes (n = 2, in duplicate; mean +/- SEM; p-Val (**)<0.01, (****)<0.0001).

Figure 6. Factors secreted by dedifferentiated melanoma cells induce YAP cytosolic translocation in mouse LN-F and decrease LN stiffness.

(A) Nude mice were injected with 501Mel CM and 1205Lu CM in the dermis of both ears. After 7 days, both draining LNs were harvested and frozen for immunofluorescence analysis. (B) Immunofluorescence analysis of YAP localization in LN-F from 501Mel CM- and 1205Lu CM-draining LN. Hoechst staining shows cell nuclei and PDGFR-β^+ delineates LN-F cytosol (Scale bar = 50 µM). Photos are 3D projections of 10 µm sections acquired in Z-stack. (C) Quantification of YAP localization in nude mice LN-F (n = 23 cells per LN and per mouse representative of 2 mice; median +/- quartiles; p-Val (****)<0.0001). (D) C57Bl/6 mice were injected with Ctrl medium and YUMM1.7 CM in the dermis of both ears. After 7 days, both draining LNs were harvested and frozen for immunofluorescence analysis. (E) Immunofluorescence analysis of YAP localization in LN-F from Ctrl and YUMM1.7 CM-draining LN. PDGFR-β^+ staining delineates LN-F cytosol, Hoechst nuclear staining was omitted for clarity reasons (Scale bar = 50 µM). Photos are 3D projections of 10 µm sections acquired in Z-stack. (F) Quantification of YAP localization in C57Bl/6 mice LN-F (n = 42 cells per LN and per mouse representative of 2 mice; median +/- quartiles; p-Val (****)<0.0001). (G) Quantification by atomic force microscopy of the stiffness of 10 µm-thick LN sections in C57Bl/6 mice, expressed as Log_{10} of the apparent Young's (elastic) modulus distribution (n = 120 measures per LN representative of 4 mice; median +/- quartiles; p-Val (****)<0.0001). Median values are 0.32 kPa for Ctrl LN and 0.21 kPa for YUMM1.7 CM-draining LN. Pictures showing LN size are above the violin plots.

Figure 7. Cytokines IL-1α and IL-1β secreted by dedifferentiated melanoma cells inhibit LN-F contractility.

(A) Antibody array analysis of 501Mel and 1205Lu CMs. IL-1α and IL-1β spots are circled in red. (B) Collagen gel contraction by LN-Fs incubated with ctrl medium, 1205Lu CM, IL-1α or IL-1β (n = 4, in quadruplicate; mean +/- SEM; p-Val (**)<0.01, (***)<0.001, (****)<0.0001). (C) ELISA analysis of IL-1α and IL-1β in melanoma CMs (n = 2, in duplicate; mean +/- SEM; p-Val (**)<0.01). (D) Spearman correlation analysis between IL-1α and IL-1β measured in melanoma CMs in (E) and contraction of LN-Fs treated with melanoma CMs. (E) Immunoblot analysis of LN-Fs treated for 5 days with Ctrl medium, 1205Lu CM, IL-1α (2 ng/ml), IL-1β (2 ng/ml) or Ruxolitinib (10 µM). HSP60 is used as a loading control. (F) Spearman correlation analysis between *MITF* expression and *IL1A* or *IL1B* expression in melanoma samples from patients (skin cutaneous melanoma TCGA dataset).

Figure 8. LN-F reprogrammed by dedifferentiated melanoma cells promote melanoma cell invasiveness.

(A) Representative 3D projections of collagen gels remodeled previously by LN-F treated with Ctrl medium, melanoma CM, IL-1β (2 ng/ml) or Y-27632 (10 µM), and then invaded for 3 days by 1205Lu Red cells. Colors indicate the distance browsed by 1205Lu Red cells on the z axis (Scale bar = 25 µm; n=2 in triplicate, 2 stacks/sample). (B) Distribution (%) of 1205Lu Red cells along the z axis in LN-F remodeled collagen gels (mean +/- SEM). (C) Percentage of 1205Lu Red cells that invaded LN-F remodeled collagen gels above 30 µm (mean +/- SEM ; p-Val (*)<0.05). (D) Maximum distance reached along the z axis by the 5% most invasive 1205Lu Red cells in LN-F remodeled collagen gels (mean +/- SEM).

Fig 1

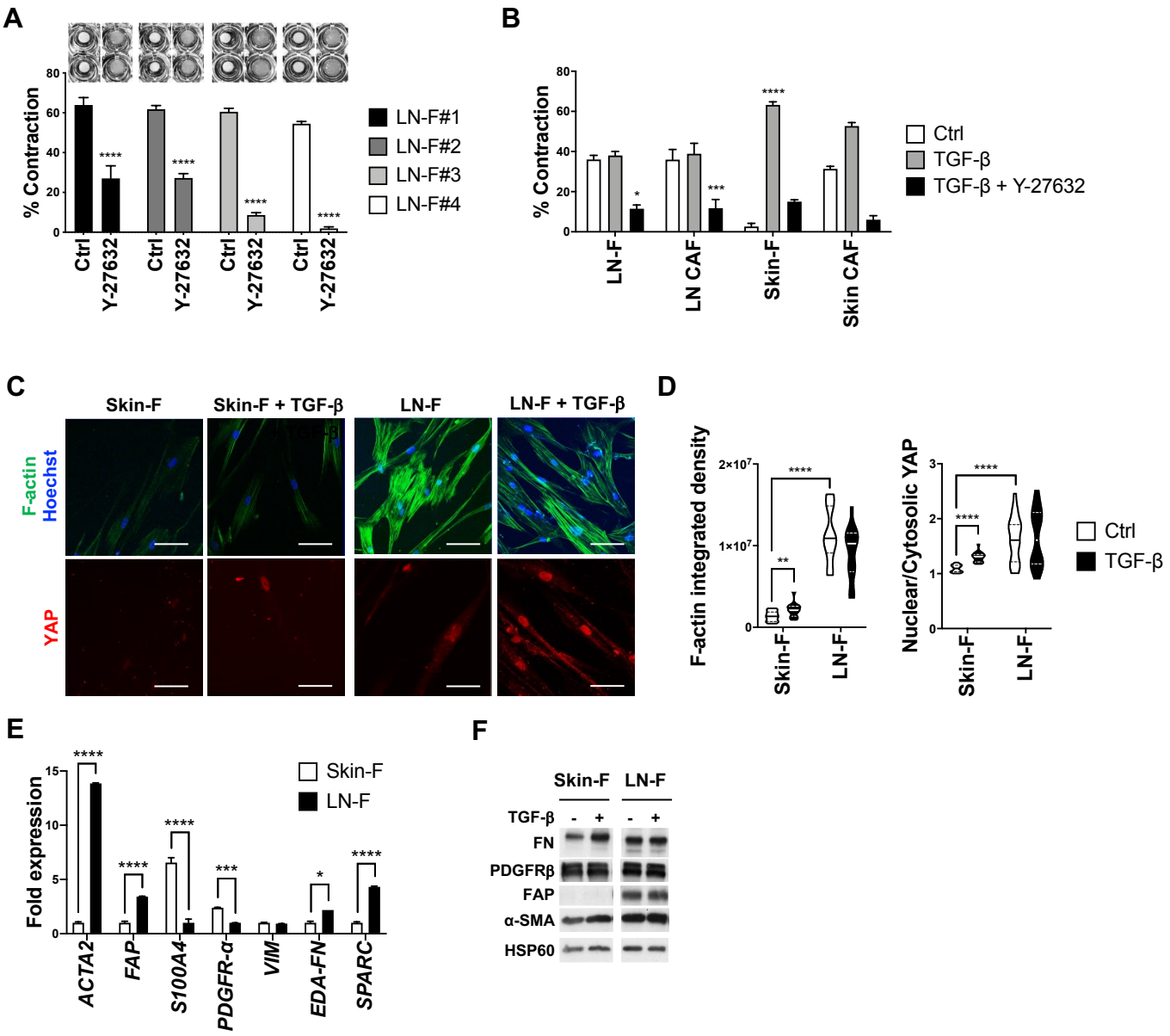
A
% Contraction
LN-F#1
LN-F#2
LN-F#3
LN-F#4
Ctrl
Y-27632
B
% Contraction
Ctrl
TGF-β
TGF-β + Y-27632
LN-F
LN CAF
Skin-F
Skin CAF
C
Skin-F
Skin-F + TGF-β
LN-F
LN-F + TGF-β
F-actin
Hoechst
YAP
D
F-actin integrated density
Nuclear/Cytosolic YAP
Ctrl
TGF-β
Skin-F
LN-F
E
Fold expression
Skin-F
LN-F
ACTA2
FAP
S100A4
PDGFR-α
VIM
EDA-FN
SPARC
F
Skin-F
LN-F
TGF-β
FN
PDGFRβ
FAP
α-SMA
HSP60

Fig 2

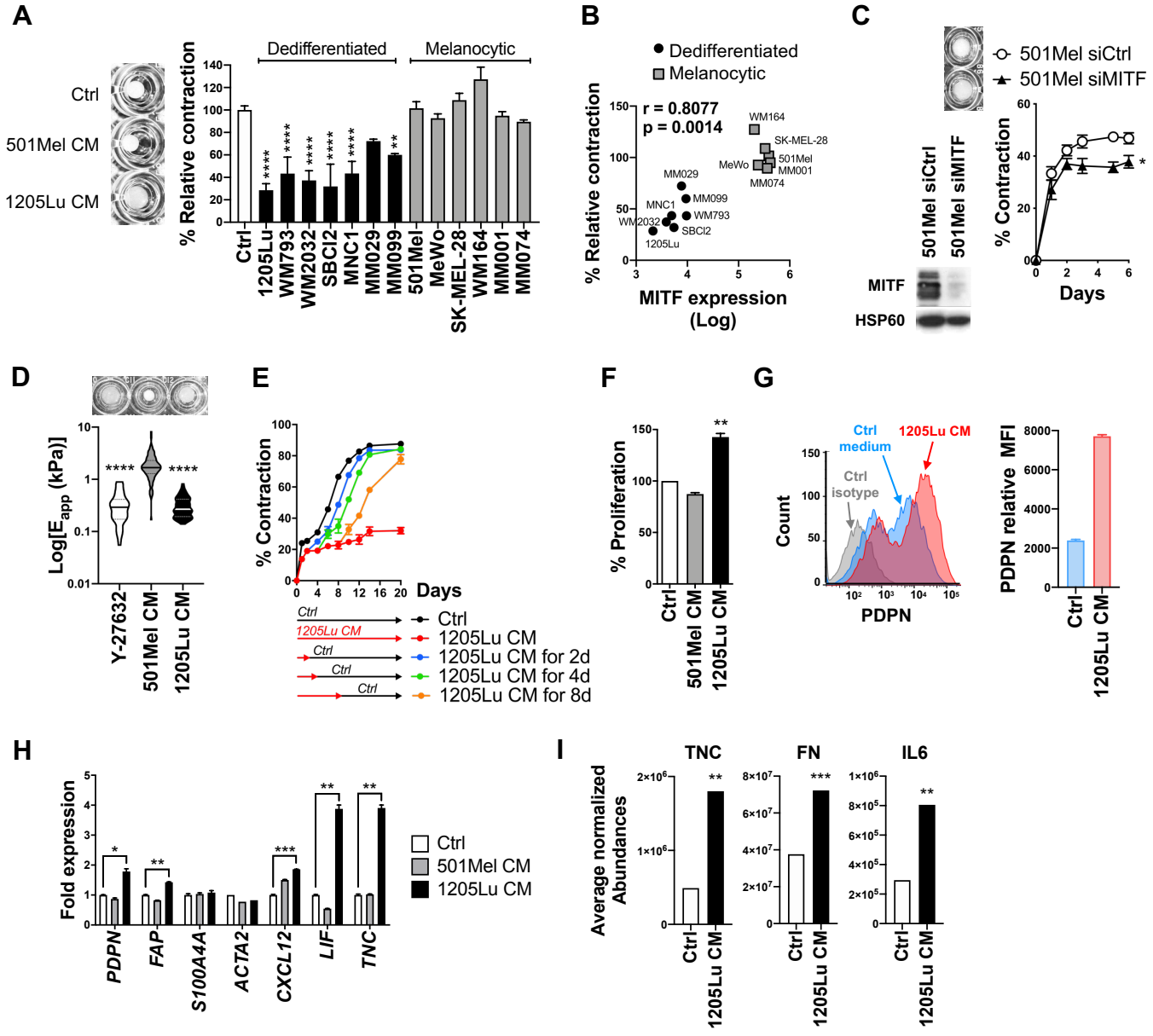
A
Ctrl
501Mel CM
1205Lu CM
% Relative contraction
Dedifferentiated
Melanocytic
Ctrl
1205Lu
WM793
WM2032
SBCl2
MNC1
MM029
MM099
501Mel
MeWo
SK-MEL-28
WM164
MM001
MM074
B
Dedifferentiated
Melanocytic
% Relative contraction
r = 0.8077
p = 0.0014
MITF expression (Log)
C
501Mel siCtrl
501Mel siMITF
% Contraction
Days
MITF
HSP60
D
Log[E_app (kPa)]
Y-27632
501Mel CM
1205Lu CM
E
% Contraction
Days
Ctrl
1205Lu CM
1205Lu CM for 2d
1205Lu CM for 4d
1205Lu CM for 8d
F
% Proliferation
Ctrl
501Mel CM
1205Lu CM
G
Ctrl medium
1205Lu CM
Ctrl isotype
Count
PDPN
PDPN relative MFI
H
Fold expression
PDPN
FAP
S100A4A
ACTA2
CXCL12
LIF
TNC
Ctrl
501Mel CM
1205Lu CM
I
TNC
FN
IL6
Average normalized Abundances
Ctrl
1205Lu CM

Fig 3

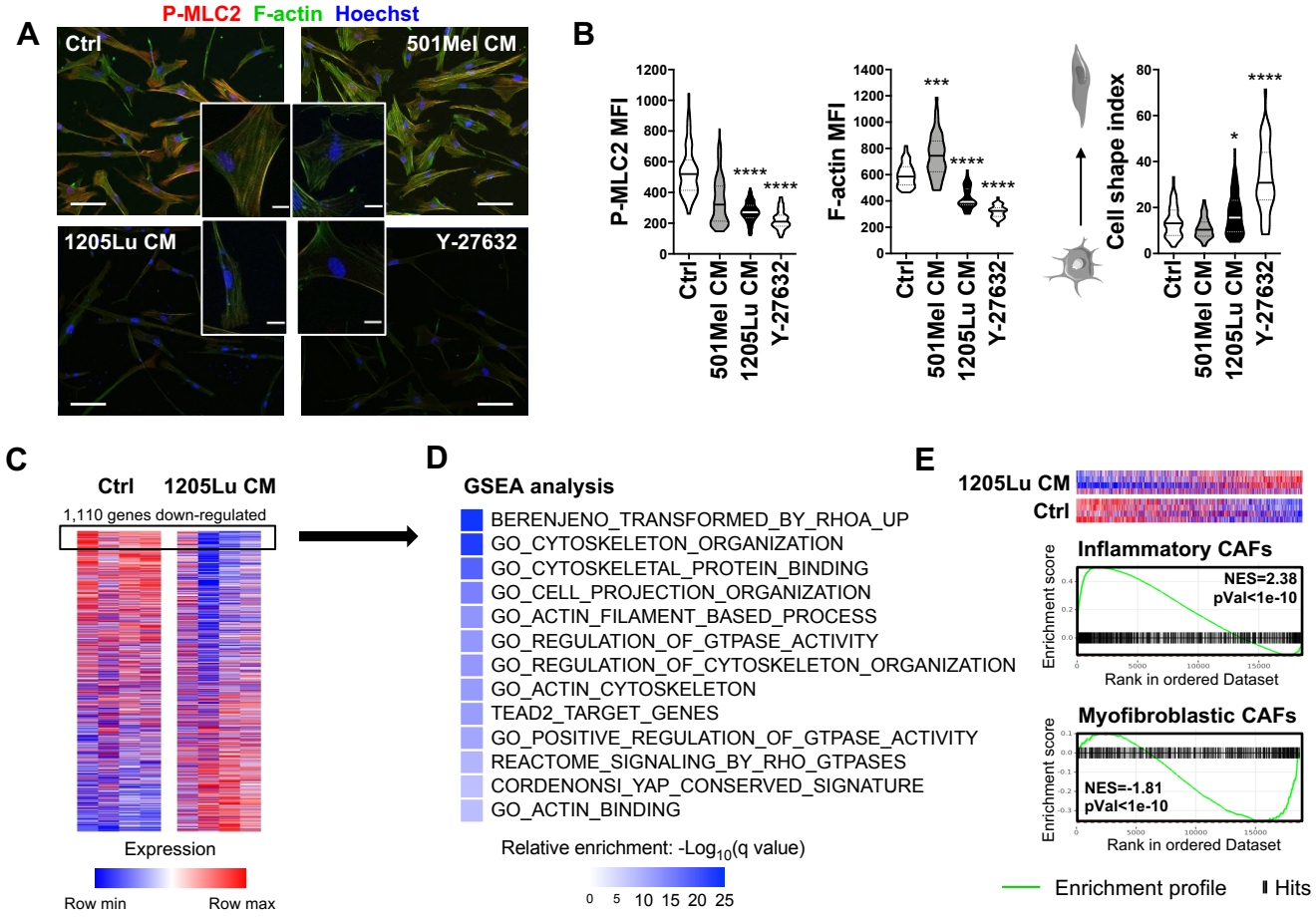
A
P-MLC2 F-actin Hoechst
Ctrl
501Mel CM
1205Lu CM
Y-27632
B
P-MLC2 MFI
F-actin MFI
Cell shape index
Ctrl
501Mel CM
1205Lu CM
Y-27632
C
Ctrl
1205Lu CM
1,110 genes down-regulated
Expression
Row min
Row max
D
GSEA analysis
BERENJENO_TRANSFORMED_BY_RHOA_UP
GO_CYTOSKELETON_ORGANIZATION
GO_CYTOSKELETAL_PROTEIN_BINDING
GO_CELL_PROJECTION_ORGANIZATION
GO_ACTIN_FILAMENT_BASED_PROCESS
GO_REGULATION_OF_GTPASE_ACTIVITY
GO_REGULATION_OF_CYTOSKELETON_ORGANIZATION
GO_ACTIN_CYTOSKELETON
TEAD2_TARGET_GENES
GO_POSITIVE_REGULATION_OF_GTPASE_ACTIVITY
REACTOME_SIGNALING_BY_RHO_GTPASES
CORDENONSI_YAP_CONSERVED_SIGNATURE
GO_ACTIN_BINDING
Relative enrichment: -Log10(q value)
0 5 10 15 20 25
E
1205Lu CM
Ctrl
Inflammatory CAFs
NES=2.38
pVal<1e-10
Enrichment score
Rank in ordered Dataset
Myofibroblastic CAFs
NES=-1.81
pVal<1e-10
Enrichment score
Rank in ordered Dataset
Enrichment profile
Hits

Fig 4

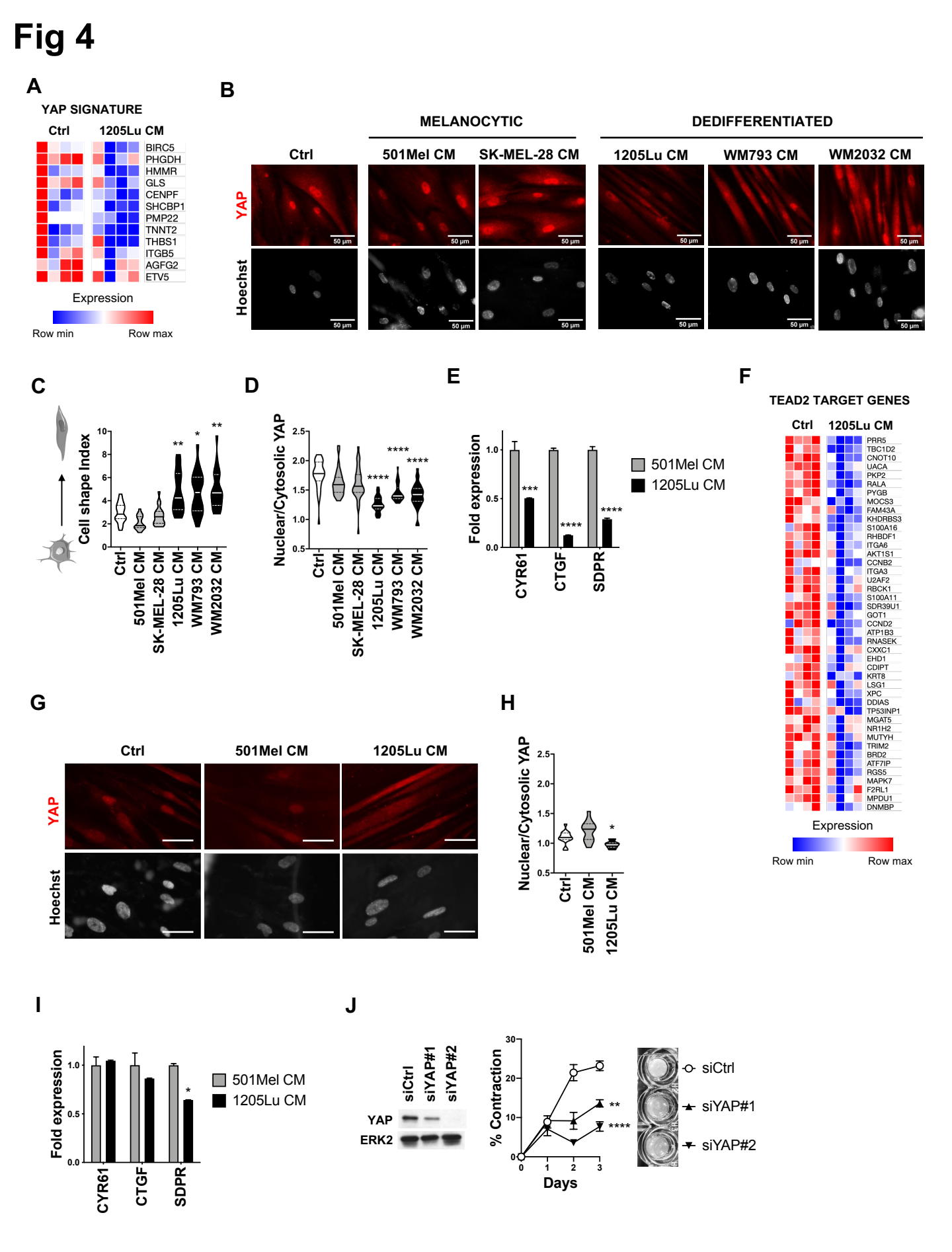
A
YAP SIGNATURE
Ctrl
1205Lu CM
BIRC5
PHGDH
HMMR
GLS
CENPF
SHCBP1
PMP22
TNNT2
THBS1
ITGB5
AGFG2
ETV5
Expression
Row min
Row max
B
MELANOCYTIC
DEDIFFERENTIATED
Ctrl
501Mel CM
SK-MEL-28 CM
1205Lu CM
WM793 CM
WM2032 CM
YAP
Hoechst
50 µm
C
Cell shape Index
Ctrl
501Mel CM
SK-MEL-28 CM
1205Lu CM
WM793 CM
WM2032 CM
D
Nuclear/Cytosolic YAP
E
Fold expression
CYR61
CTGF
SDPR
501Mel CM
1205Lu CM
F
TEAD2 TARGET GENES
Ctrl
1205Lu CM
PRR5
TBC1D2
CNOT10
UACA
PKP2
RALA
PYGB
MOCS3
FAM43A
KHDRBS3
S100A16
RHBDF1
ITGA6
AKT1S1
CCNB2
ITGA3
U2AF2
RBCK1
S100A11
SDR39U1
GOT1
CCND2
ATP1B3
RNASEK
CXXC1
EHD1
CDIPT
KRT8
LSG1
XPC
DDIAS
TP53INP1
MGAT5
NR1H2
MUTYH
TRIM2
BRD2
ATF7IP
RGS5
MAPK7
F2RL1
MPDU1
DNMBP
Expression
Row min
Row max
G
Ctrl
501Mel CM
1205Lu CM
YAP
Hoechst
H
Nuclear/Cytosolic YAP
Ctrl
501Mel CM
1205Lu CM
I
Fold expression
CYR61
CTGF
SDPR
501Mel CM
1205Lu CM
J
siCtrl
siYAP#1
siYAP#2
YAP
ERK2
% Contraction
Days
siCtrl
siYAP#1
siYAP#2

Fig 5

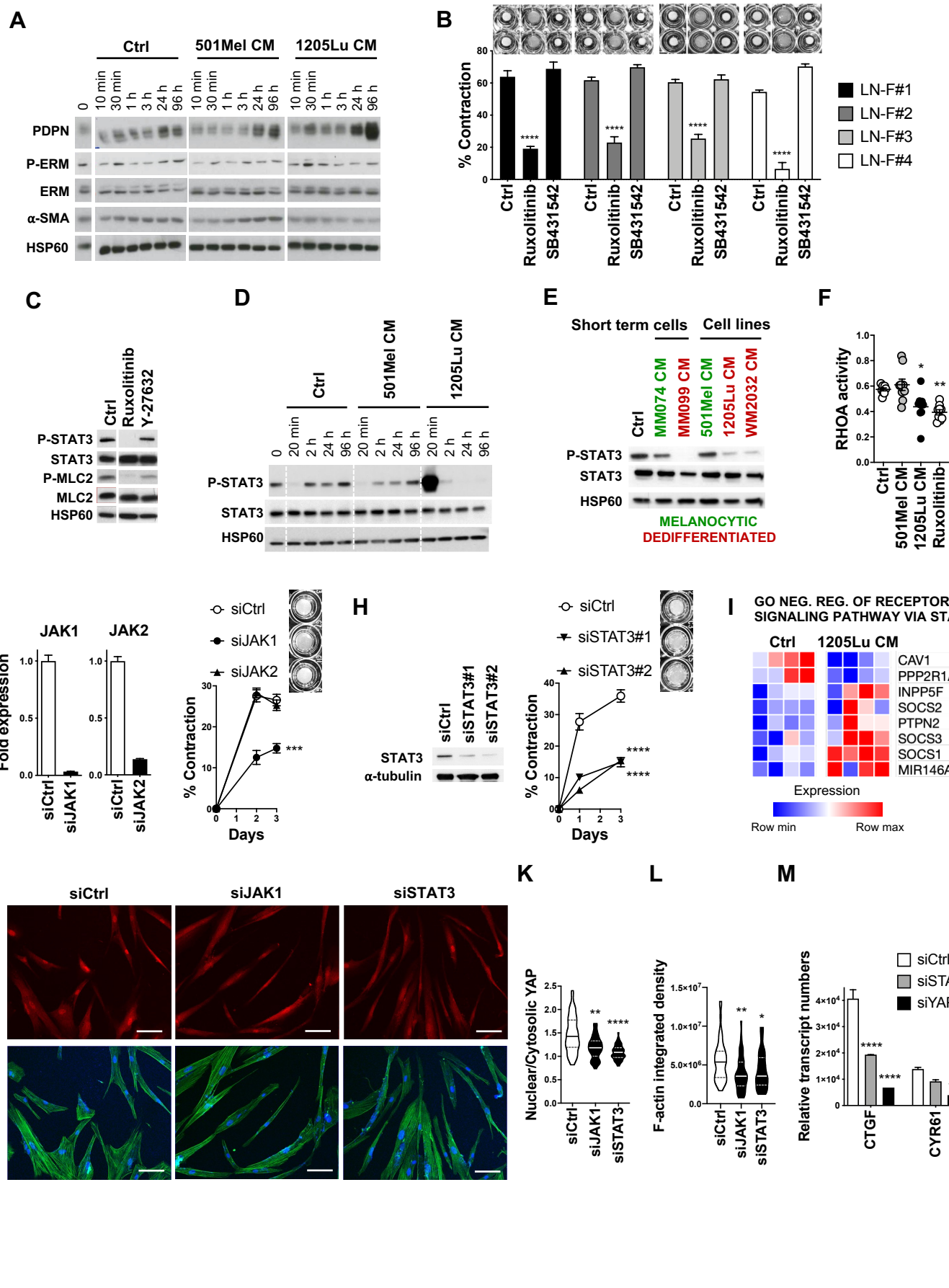
A
Ctrl
501Mel CM
1205Lu CM
0
10 min
30 min
1 h
3 h
24 h
96 h
PDPN
P-ERM
ERM
α-SMA
HSP60
B
% Contraction
Ctrl
Ruxolitinib
SB431542
LN-F#1
LN-F#2
LN-F#3
LN-F#4
C
Ctrl
Ruxolitinib
Y-27632
P-STAT3
STAT3
P-MLC2
MLC2
HSP60
D
Ctrl
501Mel CM
1205Lu CM
20 min
2 h
24 h
96 h
P-STAT3
STAT3
HSP60
E
Short term cells
Cell lines
Ctrl
MM074 CM
MM099 CM
501Mel CM
1205Lu CM
WM2032 CM
P-STAT3
STAT3
HSP60
MELANOCYTIC
DEDIFFERENTIATED
F
RHOA activity
Ctrl
501Mel CM
1205Lu CM
Ruxolitinib
G
JAK1
JAK2
Fold expression
siCtrl
siJAK1
siJAK2
% Contraction
Days
H
siCtrl
siSTAT3#1
siSTAT3#2
STAT3
α-tubulin
% Contraction
Days
I
GO NEG. REG. OF RECEPTOR SIGNALING PATHWAY VIA STAT
Ctrl
1205Lu CM
CAV1
PPP2R1A
INPP5F
SOCS2
PTPN2
SOCS3
SOCS1
MIR146A
Expression
Row min
Row max
J
siCtrl
siJAK1
siSTAT3
YAP
F-actin Hoechst
K
Nuclear/Cytosolic YAP
siCtrl
siJAK1
siSTAT3
L
F-actin integrated density
siCtrl
siJAK1
siSTAT3
M
Relative transcript numbers
siCtrl
siSTAT3
siYAP
CTGF
CYR61

Fig 6

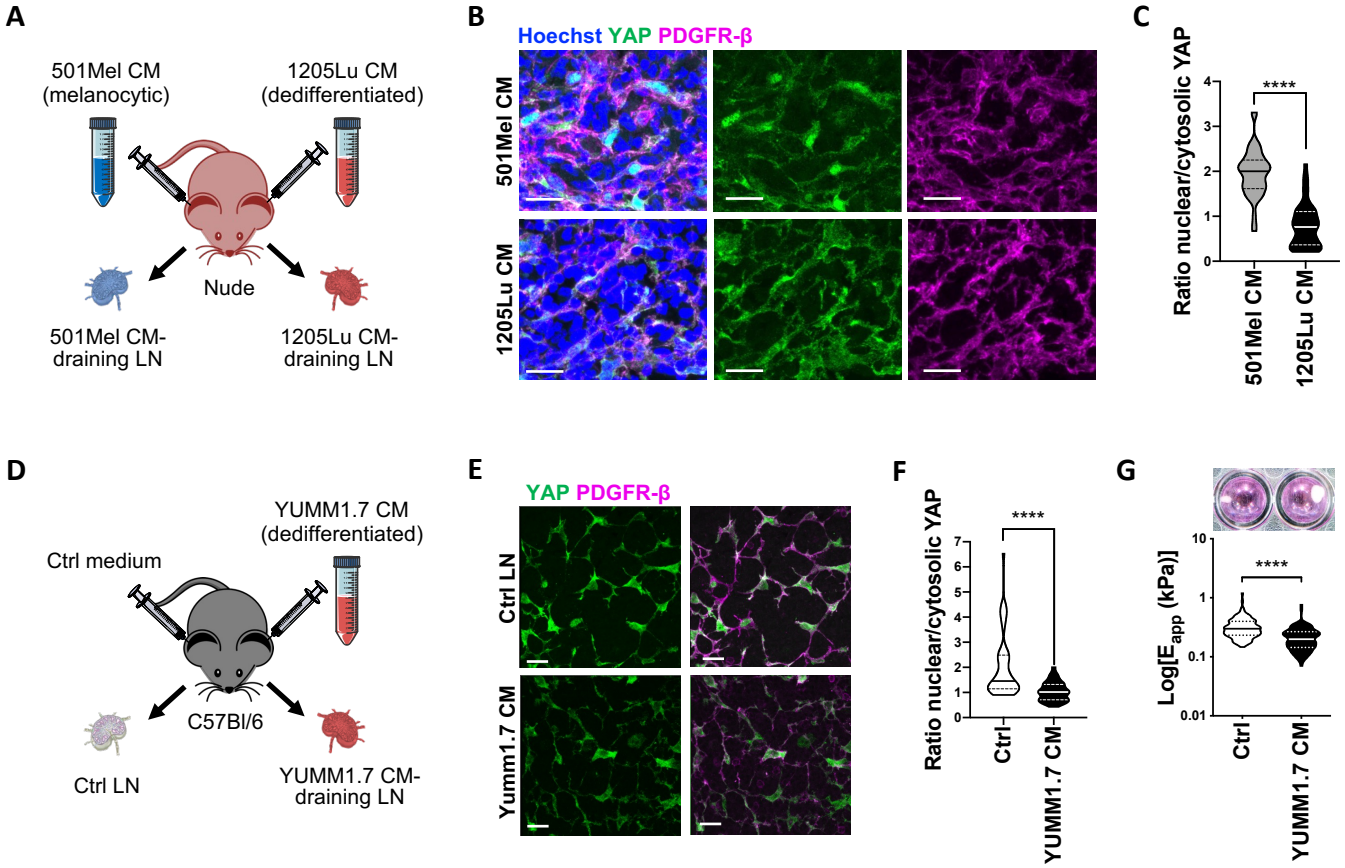
A
501Mel CM
(melanocytic)
1205Lu CM
(dedifferentiated)
Nude
501Mel CM-
draining LN
1205Lu CM-
draining LN
B
Hoechst YAP PDGFR-β
501Mel CM
1205Lu CM
C
Ratio nuclear/cytosolic YAP
****
501Mel CM
1205Lu CM
D
YUMM1.7 CM
(dedifferentiated)
Ctrl medium
C57Bl/6
Ctrl LN
YUMM1.7 CM-
draining LN
E
YAP PDGFR-β
Ctrl LN
Yumm1.7 CM
F
Ratio nuclear/cytosolic YAP
****
Ctrl
YUMM1.7 CM
G
Log[E_app (kPa)]
****
Ctrl
YUMM1.7 CM

Fig 7

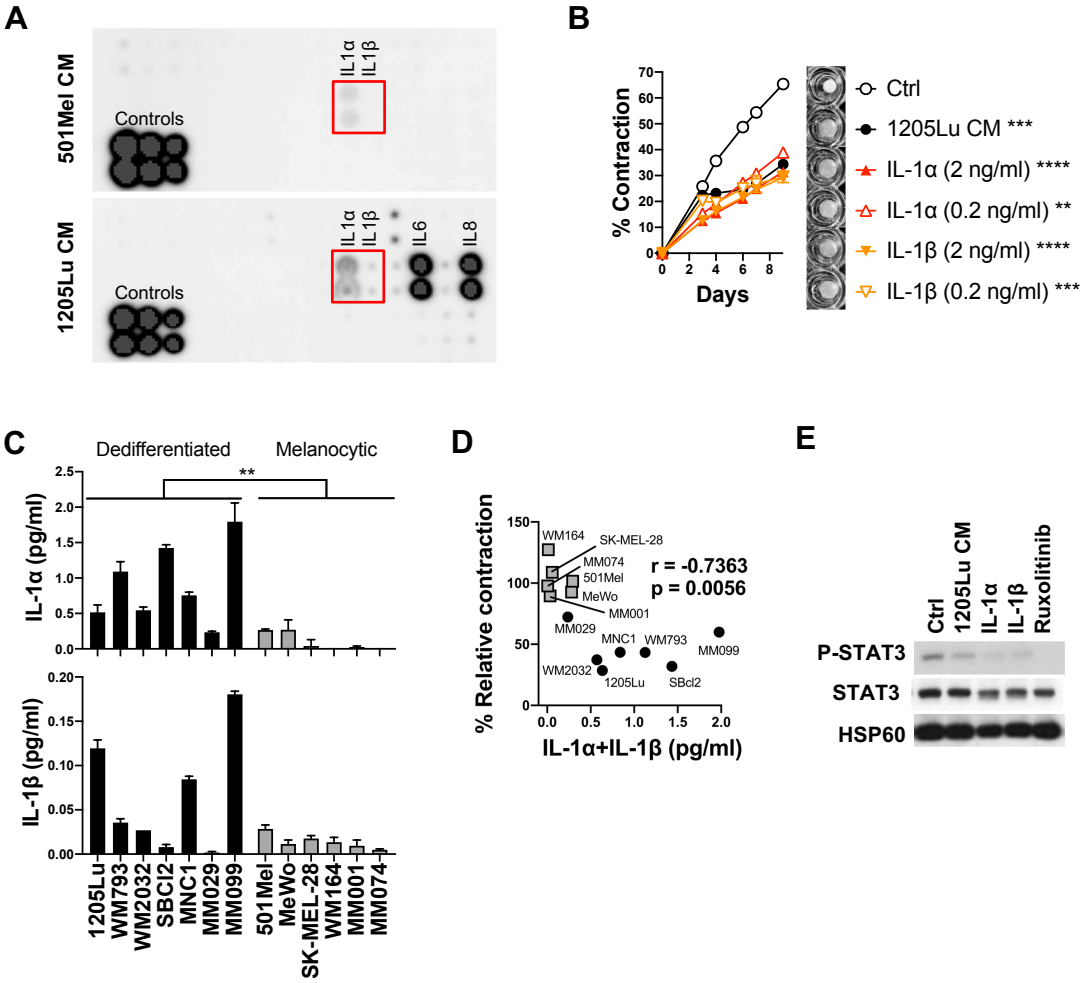
A
501Mel CM
Controls
IL1α
IL1β
1205Lu CM
Controls
IL1α
IL1β
IL6
IL8
B
% Contraction
Days
Ctrl
1205Lu CM ***
IL-1α (2 ng/ml) ****
IL-1α (0.2 ng/ml) **
IL-1β (2 ng/ml) ****
IL-1β (0.2 ng/ml) ***
C
Dedifferentiated
Melanocytic
**
IL-1α (pg/ml)
IL-1β (pg/ml)
1205Lu
WM793
WM2032
SBCl2
MNC1
MM029
MM099
501Mel
MeWo
SK-MEL-28
WM164
MM001
MM074
D
% Relative contraction
IL-1α+IL-1β (pg/ml)
r = -0.7363
p = 0.0056
WM164
SK-MEL-28
MM074
501Mel
MeWo
MM001
MM029
MNC1
WM793
MM099
WM2032
1205Lu
SBcl2
E
Ctrl
1205Lu CM
IL-1α
IL-1β
Ruxolitinib
P-STAT3
STAT3
HSP60
F
Log2 IL1A
P = 3.8e-7
r = -0.23
Log2 IL1B
P = 1.1e-8
r = -0.26
Log2 MITF

Fig 8

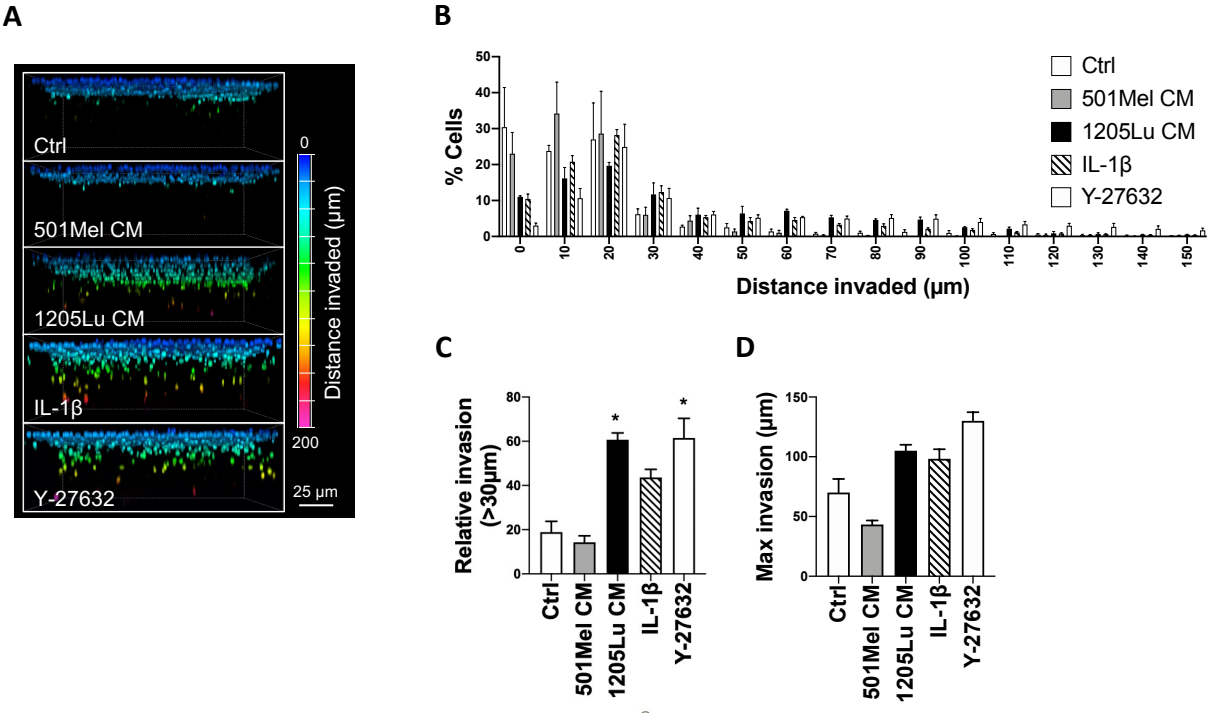
A
Ctrl
501Mel CM
1205Lu CM
IL-1β
Y-27632
0
200
Distance invaded (µm)
25 µm
B
% Cells
Distance invaded (µm)
Ctrl
501Mel CM
1205Lu CM
IL-1β
Y-27632
C
Relative invasion (>30µm)
D
Max invasion (µm)